Materials Science & Engineering C 114 (2020) 110991

Contents lists available at ScienceDirect

Materials Science & Engineering C

journal homepage: www.elsevier.com/locate/msec

Poly(3-hydroxybutyrate)/hydroxyapatite/alginate scaffolds seeded with mesenchymal stem cells enhance the regeneration of critical-sized bone defect

Alexey V. Volkov[e,g], Alexander A. Muraev[e,f], Irina I. Zharkova[a], Vera V. Voinova[a,b], Elizaveta A. Akoulina[a,b], Vsevolod A. Zhuikov[b], Dolgor D. Khaydapova[c], Dariana V. Chesnokova[a], Ksenia A. Menshikh[a], Andrej A. Dudun[a,b], Tatiana K. Makhina[b], Garina A. Bonartseva[b], Teymur F. Asfarov[e], Ivan A. Stamboliev[e], Yulia V. Gazhva[d], Valentina M. Ryabova[d], Lubomir H. Zlatev[e], Sergey Y. Ivanov[e,f], Konstantin V. Shaitan[a], Anton P. Bonartsev[a,b,*]

[a] Faculty of Biology, M.V. Lomonosov Moscow State University, Leninskie Gory 1, bld. 12, 119234 Moscow, Russia
[b] A.N.Bach Institute of Biochemistry, Research Center of Biotechnology of the Russian Academy of Sciences, Leninsky Ave. 33, bld. 2, 119071 Moscow, Russia
[c] Faculty of Soil Science, M.V.Lomonosov Moscow State University, Leninskie gory, 1, bld. 12, 119234 Moscow, Russia
[d] Privolzhsky Research Medical University of the Ministry of Health of the Russian Federation, Minin and Pozharsky Sq. 10/1, 603005 Nizhny Novgorod, Russia
[e] The Peoples' Friendship University of Russia, Miklukho-Maklaya St. 6, 117198 Moscow, Russia
[f] I.M. Sechenov First Moscow State Medical University (Sechenov University), Trubetskaya St. 8/2, 119991, Moscow, Russia
[g] N.N. Priorov National Medical Research Center of Traumatology and Orthopedics of the Ministry of Health of the Russian Federation, Priorova Str. 10, 127299 Moscow, Russia

ARTICLE INFO

Keywords:
Critical-sized bone defect
Mesenchymal stem cells
Poly(3-hydroxybutyrate)
Hydroxyapatite
Alginate
Hybrid scaffolds

ABSTRACT

A critical-sized calvarial defect in rats is employed to reveal the osteoinductive properties of biomaterials. In this study, we investigate the osteogenic efficiency of hybrid scaffolds based on composites of a biodegradable and biocompatible polymer, poly(3-hydroxybutyrate) (PHB) with hydroxyapatite (HA) filled with alginate (ALG) hydrogel containing mesenchymal stem cells (MSCs) on the regeneration of the critical-sized radial defect of the parietal bone in rats. The scaffolds based on PHB and PHB/HA with desired shapes were prepared by two-stage salt leaching technique using a mold obtained by three-dimensional printing. To obtain PHB/HA/ALG/MSC scaffolds seeded with MSCs, the scaffolds were filled with ALG hydrogel containing MSCs; acellular PHB/ALG and PHB/ALG filled with empty ALG hydrogel were prepared for comparison. The produced scaffolds have high porosity and irregular interconnected pore structure. PHB/HA scaffolds supported MSC growth and induced cell osteogenic differentiation in a regular medium in vitro that was manifested by an increase in ALP activity and expression of the CD45 phenotype marker. The data of computed tomography and histological studies showed 94% and 92%, respectively, regeneration of critical-sized calvarial bone defect in vivo at 28th day after implantation of MSC-seeded PHB/HA/ALG/MSC scaffolds with 3.6 times higher formation of the main amount of bone tissue at 22–28 days in comparison with acellular PHB/HA/ALG scaffolds that was shown at the first time by fluorescent microscopy using the original technique of intraperitoneal administration of fluorescent dyes to living postoperative rats. The obtained in vivo results can be associated with the MSC-friendly microstructure and in vitro osteogenic properties of PHB/HA base-scaffolds. Thus, the obtained data demonstrate the potential of MSCs encapsulated in the bioactive biopolymer/mineral/hydrogel scaffold to improve the bone regeneration process in critical-sized bone defects.

Abbreviations: PHB, poly(3-hydroxybutyrate); PHAs, polyhydroxyalkanoates; HA, hydroxyapatite; ALG, alginate; MSCs, mesenchymal stem cells; DICOM, Digital Imaging and Communications in Medicine; CT, computed tomography; SEM, scanning electron microscopy; WFLM, wide-field light microscopy; DSC, differential scanning calorimetry; ALP, alkaline phosphatase

* Corresponding author at: Faculty of Biology, M.V.Lomonosov Moscow State University, Leninskie Gory 1, bld. 12, 119236 Moscow, Russia.
E-mail address: ant_bonar@mail.ru (A.P. Bonartsev).

https://doi.org/10.1016/j.msec.2020.110991
Received 12 February 2020; Received in revised form 8 April 2020; Accepted 18 April 2020
Available online 25 April 2020
0928-4931/

1. Introduction

Mesenchymal stem cells (MSCs) are multipotent progenitor stem cells that can differentiate into multiple mesenchyme cell types, including fibroblasts, osteoblasts, chondrocytes, adipocytes, and myoblasts, and thus contribute to the regeneration of mesenchymal tissues such as bone, cartilage, muscle, ligament, tendon, adipose, and stroma. MSCs can be used in various clinical applications as a promising cell therapeutic product for transplantation approaches. In contrast to specialized cells (fibroblasts, osteoblasts, and chondrocytes), the use of MSCs enables the replacement of deficient endogenous cells during degenerative or regenerative processes and the renewal of cells with high proliferative potential, and causes adequate responses of the immune system after their transplantation in vivo. Studies involving a variety of animal models demonstrated that MSCs could be applied to the repair or regeneration of damaged bone, cartilage, skin, or myocardial tissues. Because of these properties, MSCs are now considered one of the most promising cell types in the field of tissue engineering [1,2].

Tissue engineering is a fundamentally different paradigm compared to surgery and transplantation. It is based not on the approaches of substitution or functional compensation of tissue, but on tissue regeneration, in which the organism itself can repair the damaged tissue if the appropriate conditions are provided. Nowadays, the study of MSCs for bone regenerative medicine and bone tissue engineering is the most rapidly growing research area. There are a number of clinical conditions, such as trauma, skeletal abnormalities, infection, osteoporosis, tumor resection, chronic inflammatory injury, and necrosis that involve bone defects. Currently, in most of these conditions, autologous bone grafting is employed as the gold standard treatment. However, this conventional technique has substantial drawbacks, such as limited graft availability and significant donor-site morbidity. To overcome these problems, bone tissue engineering with the use of MSCs and scaffolds may be a promising alternative [3,4].

The scaffolds are required as a temporary substrate for cell guidance and extracellular matrix deposition. To best mimic bone tissue, the scaffolds used in tissue engineering should have a three-dimensional (3D) microstructure with interconnected porosity and appropriate pore size, the appropriate surface microstructure, biocompatibility, and appropriate mechanical properties. It is necessary to provide intercellular fluid circulation, favorable cell attachment, migration, proliferation, and differentiation, and optimal integration with the surrounding tissue. There are different techniques to manufacture scaffolds with desired microstructure: electrospinning, salt leaching, gas foaming, particle aggregation, freeze drying, thermally induced phase separation, micromolding, microfiber wet-spinning, rapid prototyping (including 3D printing) [5–7]. 3D printing is one of the most intensive development techniques as it allows producing scaffolds with a desired shape, microstructure, and physicochemical properties. However, the development of direct 3D printing of polymer scaffolds is complicated by the fact that the materials that are traditionally employed to replace bone defects, chemically synthetic or natural polymers (polyhydroxyalkanoates (PHAs), including polylactides, polyglycolide, and its copolymers, poly-ε-caprolactone etc.), ceramics/mineral materials (hydroxyapatite, bioglass 45S5, zirconium dioxide), and xeno- and allomaterials are either not suitable for traditional 3D printing or change their physicochemical and biological properties and become unsuitable for bone reconstruction [8]. Therefore, the choice of materials in the manufacturing of devices with preselected shapes using indirect 3D technologies is also of immense importance. Such materials should provide a preselected product microstructure, as well as its physical-chemical and biological parameters (sufficient solidity, plasticity, hydrophilic properties, biodegradability, and biocompatibility).

Biodegradable and biocompatible polymers, PHAs, having a natural or synthetic origin are believed to be one of the most promising biomaterials to develop scaffolds for bone regeneration [5,9,10]. However, a single material will not always have the combination of all these properties. Therefore, in recent years, there has been active development of technologies for the manufacture of scaffolds from copolymers, blends, and composites of PHAs using different biopolymers and mineral substances [8,9,11]. A copolymerization of PHAs with other polymers allows improving their mechanical properties and hydrophilicity. So, PHAs can be chemically modified with polyurethane and 2-amino-ethyl methacrylate [12], which resulted in improvement of the mechanical properties of the prepared copolymer scaffolds. PHAs structure can be modified by gamma irradiation instead of chemical reaction and produce pure graft copolymers which also allows to change mechanical and biological properties in favor of application [13,14].

Production of composites [15] from PHAs with other biomaterials is another promising approach to develop scaffolds with superior physicochemical and biological properties [5]. Development of particulate composites [15] of PHAs with mineral biomaterials (HA [16,17] or bioglass [6,18,19] for scaffold preparation allows to regulate mechanical properties, hydrophilicity, rate of biodegradation of the composite scaffolds due to combination of each material physicochemical and biological properties, and so it can control their interaction with cells. Hydroxyapatite is widely used as bone substitute because of its biocompatibility and osteoinductivity, leading to bone regeneration in short periods of time. Hydroxyapatite has a chemical and structural similarity to the mineral phase of native bone [20,21]. However, HA scaffolds and other devices showed low modulus of elasticity and fracture toughness, which limits its application to bone tissue engineering. And for that reason it cannot be used for load-bearing functions in large bone defects, and it is used mostly in granules and bulk forms [20]. Therefore, the approach to use scaffolds on the basis of polymer-HA composites can be particularly promising [5,21,22]. The blending polymers with HA can be used also for development of sustained drug release systems [23].

However, regarding the direct and indirect 3D-printing [8] the most challenging way is to develop complex multidirectional continuous fiber composites [15], in which the reinforcement and the matrix would be represented by completely different materials in their physicochemical properties. This is the most biomimetic structure of composites: sporocarp, wood, endocarp, coral, sponge, nacre, skin, cartilage, bone are composites consisting of the stiff reinforcement impregnated with a hydrogel-like matrix. The composites of precisely this structure create the most natural environment for cell growth inside them [24].

In addition to PHAs, hydrogels are also often used for bioengineering of hard connective tissue, first of all, alginate(ALG)-based hydrogels [5,9,10,25]. PHAs and ALG have very different properties, in that PHAs are hydrophobic, mechanically strong, and slowly biodegradable polyesters, while ALGs are hydrophilic, hydrogel-forming, mechanically destructible, and rapidly biodestructible polysaccharides. The generation of composites from polymers of these two classes makes it possible to adjust the properties of the resulting composite material very widely. ALGs are frequently used for the manufacture of scaffolds in bone, cartilage, soft connective, and muscular tissue engineering [25], while PHA-based scaffolds are mostly employed for bone tissue regeneration [9]. PHAs, in particular homopolymer poly(3-hydroxybutyrate) (PHB), is generated biotechnologically using the highly effective producer strain *Azotobacter chroococcum* 7B, which enables the acquisition of high-purity polymers with the desired properties [26]. Moreover, natural biodegradable PHB has good biocompatibility, osteoconductive, and even osteoinductive properties, whereas chemically synthetic PHAs: polylactides, polyglycolides and their copolymers can cause during their biodegradation local pH decrease at the implantation site, which leads to the development of a chronic inflammatory reaction [27,28]. Even though ALGs for biomedical purposes are derived from brown algae, these polymers can also be obtained by biotechnology using producer strains of the same bacteria genus *Azotobacter* [29]. It was shown that ALG can be used for the encapsulation of stem cells and

chondrocytes in porous scaffolds from chemically synthetic PHAs (polycaprolactone and polylactide-*co*-glycolide) to produce hybrid constructions for tissue engineering [30,31]. But the biomimetic composite structures from natural PHB (and its composites) as reinforcement and ALG as matrix were not earlier used for the development of MSC-seeded tissue engineering constructions for bone tissue regeneration and their osteoinductive potential was not evaluated.

Thus, the purpose of this study is to investigate the effect of the hybrid composite constructions based on PHB/HA scaffolds filled with ALG hydrogel seeded with MSCs on the regeneration of the critical-sized radial defect of the parietal bone in rats.

2. Materials and methods

2.1. Animals and ethics statements

All experiments and surgical procedures were performed in accordance with the ethical guidelines issued by the ISO 10993-1:2009 and approved by the local Bioethics Committees of Peoples' Friendship University of Russia Laboratory Animal Ethics Committee of the PLA Navy General Hospital. Surgical procedures were carried out on 24 adult male Wistar rats weighing 350 g. All rats were housed in a stable animal care room with suitable temperature and humidity and a 12/12 h light/dark cycle; they had free access to food and water throughout the experiment. Scaffold experimental investigation was performed in accordance with a widely used multidisciplinary experimental design for research in biomaterials and tissue engineering areas including scaffold preparation, study of morphology and physicochemical properties, study of cell growth in vitro, and in vivo study using tissue defect model on laboratory animals [4,5,9,11].

2.2. Isolation, culturing, and characterization of MSCs

The MSCs were isolated from the femurs of young (3–5 days old) Wistar rats and cultured for 2 weeks in Dulbecco's modified Eagle medium (DMEM, PanEco, Russia) supplemented with 10% fetal calf serum (FCS, Biological Industries, Israel), 100 U/ml penicillin. For the characterization of the cell phenotype, we used MSC culture on the third passage. The cells were removed by incubation in a solution of trypsin-versene for 5 min and counted using a hemocytometer. Then, a suspension of 10^5 cells in 100 μl of PE buffer (2 ml EDTA-0.5% ETS in phosphate buffered saline (PBS)) was prepared and incubated with antibodies to CD90 and CD29 (eBioscience, USA) as the most relevant positive markers of the MSC phenotype, and to CD45 and CD11b/c (eBioscience, USA) as the most relevant negative surface markers of the MSC phenotype (eBioscience, USA) [32,33] in the dark for 40 min at a temperature of 5 °C. To estimate viable cells in the MSC population, the vital marker 7-Aminoactinomycin D (7AAD) was used. Cells were washed by centrifugation once in PBS and were analyzed on a flow cytometer (FACS ARIA II, USA). The analysis of results and construction of graphs were performed using the program Flowing Software 2.5.1 (Supplemental materials, Fig. S1) [34].

2.3. Scaffold preparation and characterization

2.3.1. Biomaterials for scaffold production

PHB (molecular weight (Mw) = 1.5×10^5) was produced by employing an original biotechnological technique using a highly productive strain-producer of PHB *Azotobacter chroococcum* 7B. Then, the polymer was isolated and purified for biomedical application; PHB M_w was determined through viscosimetry, as previously described [26]. The powder of PHB was produced using Nano Spray Drier B-90 (Buchi, Switzerland). Sodium ALG and hydroxyapatite (HA) (with particles of size < 1 μm) were purchased in Merck (former Sigma-Aldrich, Germany), and were used as received. FTIR spectra that confirm chemical structure of PHB and ALG are presented in Supplemental materials, Fig. S2.

2.3.2. Computer modeling and 3D printing of molds for scaffolds with desired shape manufacturing

Cone Beam Computed Tomography of the rat's head was performed. A 3D model of the skull was reformed based on Digital Imaging and Communications in Medicine (DICOM) files. A cylindrically shaped bone defect that was 8 mm in diameter was simulated on the center of the parietal bone. The implant model was manufactured so that it not only filled the bone defect, but also overlapped it on the outside. This enables the protection of the dura mater and the brain from external effects. The study was performed on rats of equal weight and size, all models were also manufactured to have the same size (Supplemental materials, Fig. S3A,B) [8,35].

2.3.3. Manufacture of scaffold molds using 3D printing

The scaffold molds were manufactured from polylactide using a 3D printer PrusaMendel v2 (NWRepRap, USA) based on the principle of fused deposition modeling. The molds were isolated with aluminum foil as organic solvent chloroform dissolving polylactide was used in the process of mold manufacturing. The process of implant molding is easily scaled for manufacturing implants that are up to 5 × 5 × 5 cm in size (Supplemental materials, Fig. S3C,D) [8,35].

2.3.4. Porous composite scaffold production

We prepared the scaffolds using the salt double-leaching porosity-control technique, which is a modification of the salt leaching methods that are widely applied in tissue engineering [5,8,36,37] using two different porogens, namely ammonium carbonate and sucrose with crystals of desired size.

Ammonium carbonate was used as a porogen owing to its unique potential to decompose in dry conditions and by hydrolysis in water solutions at a high temperature (> 60 °C) with the production of gases and water without any impurities:

$$(NH_4)_2CO_3 \rightarrow 2NH_3 \uparrow + CO_2 \uparrow + H_2O,$$

$$(NH_4)_2CO_3 + 2H_2O \leftrightarrow 2NH_4OH + H_2CO_3 \rightarrow 2NH_3 \uparrow + CO_2 \uparrow + 3H_2O.$$

The sucrose was used as a conventional leaching agent.

To produce pores in scaffolds with different diameters, we used the crystals of sucrose (Sigma-Aldrich, Germany) and ammonium carbonate (Khimmed, Russia) with the desired size. For this purpose, the purchased substances of sucrose and ammonium carbonate were initially sieved through laboratory pharmaceutical sieves U1-ESL (Kraft, Russia) with mesh sizes of 94 and 315 μm. Then, a solution of PHB in chloroform or 10% (w/v) suspension of HA in the PHB chloroform solution (EKOS-1, Russia), 60 mg/ml was mixed layer-by-layer with the sifted crystals of sucrose and ammonium carbonate in a ratio of 6:1:1 (w/w) in a Petri dish. The manufactured molds were filled with the properly mixed dispersion of porogens in PHB solution or PHB/HA suspension and were left to evaporate the solvent. Then, the samples were placed in hot water (~65 °C) to produce porosity both by the release of gas and sucrose leaching. After gas formation stopped, the obtained scaffold was washed 5 times in distilled water and dried for about 24 h at 20 °C [34,35]. ALG hydrogel (e.g. containing MSCs) in the form of granules (spheres) was prepared by the pipetting of 1% sodium ALG solution into a 50-mM solution of $CaCl_2$ until the complete gelling of ALG, after which the obtained hydrogel spheres were washed with PBS. The PHB and PHB/HA scaffolds and ALG hydrogel were used in experiments for the study of MSC proliferation and differentiation in vitro.

For in vivo experiments, the composite PHB/ALG, PHB/HA/ALG, and hybrid PHB/HA/ALG/MSCs scaffolds were produced. To obtain PHB/ALG and PHB/HA/ALG scaffolds, the mold-producing PHB and PHB/HA scaffolds were filled with 1% ALG solution until full saturation. Then, they were placed in a 5% (w/v) solution of $CaCl_2$ until the complete gelling of ALG in the scaffold, after which the obtained

composite scaffolds were washed with PBS. The produced scaffolds have the same size: plug disc of 8 mm in diameter, cap disc of 12 mm in diameter, 2 mm thick.

Such hybrid scaffold construction based on PHB filled with sodium ALG was developed considering previously obtained data [35]. Sodium ALG can be further employed for the encapsulation and introduction of mesenchymal stem cells as well as other cells used to stimulate bone and cartilage tissue regeneration in the scaffold [30,31,38].

2.3.5. Production of hybrid scaffold seeded with MSCs

Before filling the PHB and PHB/HA porous scaffolds with hydrogel, the bone marrow MSCs were embedded in the sodium ALG solution, which is used as a vehicle for MSC encapsulation in the scaffolds [30,31,38]. For this purpose, sodium ALG powder, which was sterilized in ethanol and under UV irradiation, was dissolved for 6 h with stirring on a magnetic stirrer in saline in a 1% (w/v) concentration under aseptic conditions. Then, a suspension of MSCs at a concentration of 200,000 cells per 1 ml in the obtained ALG solution was prepared (the final concentration of ALG was 1.0% (w/v)). The PHB and PHB/HA scaffolds produced earlier were impregnated with the resulting suspension by an automatic pipette with 100 μl (20,000 cells) suspensions per sample. After impregnation, the excess ALG solution was removed and poured with a sterile 5 mM $CaCl_2$ solution to obtain the ALG hydrogel-containing cells. After incubation for 3 min in calcium chloride, the scaffolds were washed in phosphate buffer.

2.4. Scaffold characterization

2.4.1. Porosity

The following equations were used to calculate the porosity of PHB and PHB/HA scaffolds:

$$D = \frac{m}{h \times l \times w} \tag{1}$$

where D is the apparent density (g/cm^3), h is the height (or thickness) (cm), l is the length (cm), w is the width (cm), and m is the mass (g) of the scaffold.

$$P = \left(1 - \frac{D}{d}\right) \times 100\% \tag{2}$$

where P (%) is the porosity, d is a theoretical value of the bulk density of the scaffold as a monolithic sample without pores (g/cm^3), and D is the apparent density, which is calculated by Eq. (1) (g/cm^3).

The value of the bulk density of the PHB/HA 90:10 blend is 1.437 g/cm^3, considers the bulk density 1.243 g/cm^3 for PHB and 3.180 g/cm^3 for HA. The weight of samples was measured using the laboratory scale AL-64 (Acculab, USA). The height, length, and width of the scaffold samples were measured using the caliper (Krino, Italy).

2.4.2. Morphology

We used the Cyber-shot DSC-RX100 digital camera (Sony, Japan) with a macro function to obtain images of the scaffolds. To study the morphology of the PHB and PHB/HA scaffolds, we used a wide-field light and a scanning electron microscope. Scanning electron microscopy (SEM) was used to examine the microstructure of the scaffolds. The samples of scaffold pieces of size 2 × 2 × 2 mm were mounted on aluminum stumps, coated with gold in a sputtering device (IB-3, Giko, Japan) at 15 mA for 15 min, and then examined using the scanning electron microscope (JSM-6380LA, JEOL, Japan). The diameter of micropores was calculated by Image J software using SEM images. The data were presented as an average (n = 15) [34].

The morphology of the scaffolds was also examined by wide-field light microscopy (WFLM) using the stereomicroscope Nikon SMZ1500 (Nikon, Japan). This technique was also used to determine the interconnection of pores in the scaffold samples after the ink test. The samples were immersed in the ink solution, dried, and then cross-sectioned. To ensure the absence of closed pores (which consider the cut as white spots), the ink-black color distribution in the internal volume of the samples was studied by WFLM [34].

2.4.3. Differential scanning calorimetry (DSC)

We analyzed the thermal properties of the PHB and PHB/HA scaffolds using the differential scanning calorimetry method. The samples of scaffold pieces of size 2 × 2 × 2–4 × 4 × 2 mm with a mass of about 1–4 mg was sealed in a 25 μl aluminum crucible and placed in the differential scanning calorimeter 204 F1 Phoenix (Netzsch, Germany). The samples were heated from 25 °C to 200 °C at a rate of 10 °C/min in a nitrogen atmosphere. The peak temperature of the heat capacity change was designated as the melting point T_m^{peak}. The accuracy of the measurement did not exceed 1 °C for the temperature or 1 J/g for the melting enthalpy. The crystallinity (X_c) of a PHB component was calculated by the following equation [39]:

$$X_c = \Delta H_m / \Delta H_{0m}(\text{PHB}) \tag{3}$$

for the PHB scaffold, and

$$X_c = \Delta H_m / \Delta H_{0m}(\text{PHB}) \times \omega(\text{PHB}) \tag{4}$$

for the blend PHB/HA scaffold,where H_{0m}(PHB) is the theoretical value (146.6 J/g) of the thermodynamic melting enthalpy for a 100%-crystalline PHB sample, H_m(PHB) is the apparent melting enthalpy corresponding to the PHB component, and ω(PHB) is the weight fraction of PHB in the PHB/HA blend. Data are presented as an average of three measurements. All calculations were performed for the first heating cycle.

2.4.4. Mechanics

We studied the mechanical properties of the PHB and PHB/HA scaffolds using the rheometry technique. The rheometer MCR 302 (Anton Paar, Austria) was equipped with a plate-plate measuring system. First, an amplitude test was performed to find the linear viscoelasticity range (0.04%) and the optimal gap (relative deformation 0.1–0.3) at an angular frequency of 10 rad/s. Then, a frequency test was performed on another sample at an angular frequency ranging from 0.1 to 100 rad/s. The mechanical characteristics of the scaffold samples of initial size (see Section 2.3.4) were measured by their compression. The dependence of the normal pressure on the relative strain was built. Then, Young's modulus was calculated from the slope of the linear part of the chart [34].

2.4.5. Water uptake

To evaluate the hydrophilicity of the PHB and PHB/HA scaffolds, we carried out the water uptake test [34]. The samples of scaffolds of initial size (see Section 2.3.4) were maintained at a temperature of 50 °C for 2–3 days to reach a constant value of mass (m_1). After that, they were immersed in deionized water (t = 25 °C) for 3 h. After removing the water droplets, the samples were weighed again. The water uptake of the PHB and PHB/HA scaffolds was calculated using the equation:

$$A = (m_2 - m_1)/m_1 \times 100, \tag{5}$$

where m_1 and m_2 are the masses of the dry and water-saturated scaffolds, respectively.

2.5. MSC proliferation and differentiation in vitro

2.5.1. Cell viability test

To test the ability of the PHB and PHB/HA scaffolds to maintain the growth of MSCs, we performed an XTT cell proliferation test. Each of the samples of scaffold pieces of size 5 × 5 × 2 mm was placed at the center of the well bottom of the tissue culture polystyrene (TCPS) 96-well plate. The MSCs were detached from cell culture flasks where they were previously cultivated using 0.25% w/v trypsin/0.02% EDTA

(PanEco, Russia). One hundred microliters of the cell suspension containing about 2000 cells were placed on the top of each scaffold sample. The same number of cells was embedded in a 1% solution of sodium ALG to produce spheres of ALG hydrogel containing MSCs. The ALG hydrogel spheres were obtained by pipetting the ALG solution with MSCs through the needle of the 1-ml insulin syringe to the 50-mM $CaCl_2$ solution for 1-min incubation with immediate washing of the obtained spheres in the DMEM. MSCs were cultivated for 1, 3, 7, and 14 days. The MSC growth in wells of the TCPS 96-well plate without scaffolds was studied as a control. The cell viability was examined using the cell proliferation reagent XTT according to the manual of XTT Cell Proliferation Kit (Biological Industries, Israel). The samples of the scaffolds with attached MSCs were gently and quickly transferred from wells of the TCPS plate in which they were previously incubated to the respective wells of a new TCPS plate with the initially added 100 μl of fresh DMEM. Then, 50 μl of the XTT reagent solution was added to each well. Multi-well plates were incubated at 37 °C for a further 4 h. The scaffold samples were removed, and absorbance measurements were carried out using a microplate spectrophotometer Zenyth 3100 Microplate Multimode Detector (Anthos Labtec Instruments GmbH, Austria) at 450 nm with a reference wavelength of 620 nm [34].

2.5.2. Alkaline phosphatase activity and MSC phenotype marker tests

To study the osteogenic differentiation of MSCs grown in the PHB and PHB/HA scaffolds, we analyzed the alkaline phosphatase (ALP) activity and the expression level of the CD45 marker. Before testing, the specimens of the scaffolds that were 10 × 10 mm in size were seeded with MSCs at a density of 7000 cells per sample, and MSCs were cultivated for 7, 14, and 21 days.

To measure the ALP activity in MSCs, the specimens of the scaffolds with MSCs grown in them were washed two times with PBS, placed in a lysis buffer having the following composition: 250 mM NaCl, 0.1% Triton X-100, 50 mM Hepes, and pH 7.5, and they were then subjected to three freeze-thaw cycles. Then, the obtained cell lysate samples were centrifuged at 10,000 rpm for 10 min. One hundred microliters of the cell lysate supernatant and 15 μl of the ALP activity reagent with the composition 15 mM *n*-nitrophenyl phosphate and 2 mM MgCl (pH = 10, Sigma-Aldrich, Germany) were dropped into the wells of the TCPS 96-well plate, and incubated in a thermostat at 37 °C for 120 min. Then, the optical density was measured at 405 nm. The lysis buffer served as a negative control, and MSCs grown on culture plastics without scaffolds were also used as a positive control [34]. The ALP activity is one of the main markers of MSC osteogenic differentiation [40–43].

To examine the change in the expression level of the CD45 marker, we used the immunochemistry technique. The stem cell phenotype during their cultivation in PHB and PHB/HA scaffolds was monitored on the flow cytometer (FACS ARIA II, USA) on the 6th and 14th days using the antibodies to CD45 (eBioscience, USA) [34]. The CD45 is widely used for the MSC phenotyping as a negative marker to identify MSCs of any origin (human, rat, or mouse). This marker is known as the transmembrane protein-tyrosine phosphatase (leukocyte common antigen, L-CA, B220, T200, Ly-5, EC 3.1.3.48) - a glycoprotein that present on the surface of all the representatives of the blood-forming series, except for mature erythrocytes. The absence of the surface marker CD45 in undifferentiated MSCs is mandatory [32,33].

2.6. In vivo study on critical bone defect

2.6.1. Operation technique

To study the regeneration of cranial bones, we used the model of critical-sized calvarial defect in rats. This model is used to evaluate the efficacy and biocompatibility of various bone-replacing materials, including scaffolds with growth factors and cells [44–46].

The rats were anesthetized with Zoletil 100, which was administered intraperitoneally at a dose of 125 μg/kg of body weight. A round opening was formed in the middle of the sagittal suture on a cranial vault that was 8 mm in diameter, thereby preventing the perforation of sagittal venous sinus. Then, the defect was filled with the PHB/ALG, PHB/HA/ALG or PHB/HA/ALG/MSC scaffold of initial size and design (see Section 2.3.4). The wound was sutured in layers (Supplemental materials, Fig. S7) [35].

2.6.2. Introduction of fluorescent marks to study the bone defect regeneration process

To assess the dynamics of neo-osteogenesis, an intravital triple marking of the newly formed bone tissue was performed. All experimental rats were administered with intra-abdominal injections of doxycycline solution by the beginning of active osteoid mineralization on days 8, 9, and 10 after the operation. Further, on days 15, 16, and 17 of the experiment, the rats were administrated tetracycline solution intraperitoneally, which generated a new marked area penetrating the neoformed bone tissue. On days 22, 23, and 24, alizarine red C was introduced for the complete dyeing of the edges of the mineralized regenerate. The marks were introduced in the dose of 25 mg/kg of body weight. Thus, marking was performed according to the scheme 7–3–4–3–4–3–4 (three days of introduction alternated with four-day breaks) [35].

On day 28, which corresponded to the completion of primary osteogenesis processes [47], the rats were sacrificed with an overdose of Zoletil/Rometar. The calvarium was skeletonized, and the regenerate area was harvested using surgical cylindrical drills and a console. The obtained calvarium samples were fixed in 40% ethyl alcohol for 24 h. This fixation method is widely used to retain fluorescent marking and the good saturation of bone tissue [35,48].

2.6.3. Computed tomography imaging

The obtained plastic blocks were tested using a cone beam volume CT before incising. Scanning was performed using a cone beam volume CT Point 3D Combi 500 C, (Pointnix, South Korea) in 63 kVp/7 mA mode. Using the installed software Horos Project-Free DICOM Medical Image Viewer, the area of bone defect healing was evaluated. Therefore, using the special tool of this software, the borders of the defect were outlined, and its area was automatically estimated. The restoration of the bone defect was calculated using the equation:

$$R = (a_1 - a_2)/a_1 \times 100, \quad (6)$$

where a_1 is the initial and a_2 is the current surface area of the critical bone defect, respectively [35].

2.6.4. Histological investigation

The samples were placed in 70% ethanol for 24–72 h. After that, they were washed, dehydrated, and submerged in methylmethacrylate (Osteo-Bead; Sigma-Aldrich, USA) with subsequent polymerization, according to the standard procedure recommended by the manufacturer. The obtained blocks were used to manufacture primary slices having a thickness of 200 μm (Lowspeed sow Jet; Switzerland), which generated secondary slices that were 40–50 μm in thickness. Slice thickness control was carried out using a standard mechanical drum-type micrometer. The original trichrome blue staining (orange G, eosin, toluidine blue, and basic fuchsin) was used to visualize the remodeled tissue within the bone defect area, the fibrous connective tissue, and mineralized deposits. The restoration of the bone defect was calculated using the Eq. (6) based on data on the length of the new bone covering of 8–10 cross sections [35].

2.6.5. Microscopy

Microscopic examinations were carried out using the fluorescent imaging microscope Leica DM 4000B (Leica Microsystems, Germany). Microphotography was performed using a standard set of optical filters with a subsequent combination of RGB-channels in a single image using the standard Leica software product for fluorescence microscopy (multi-

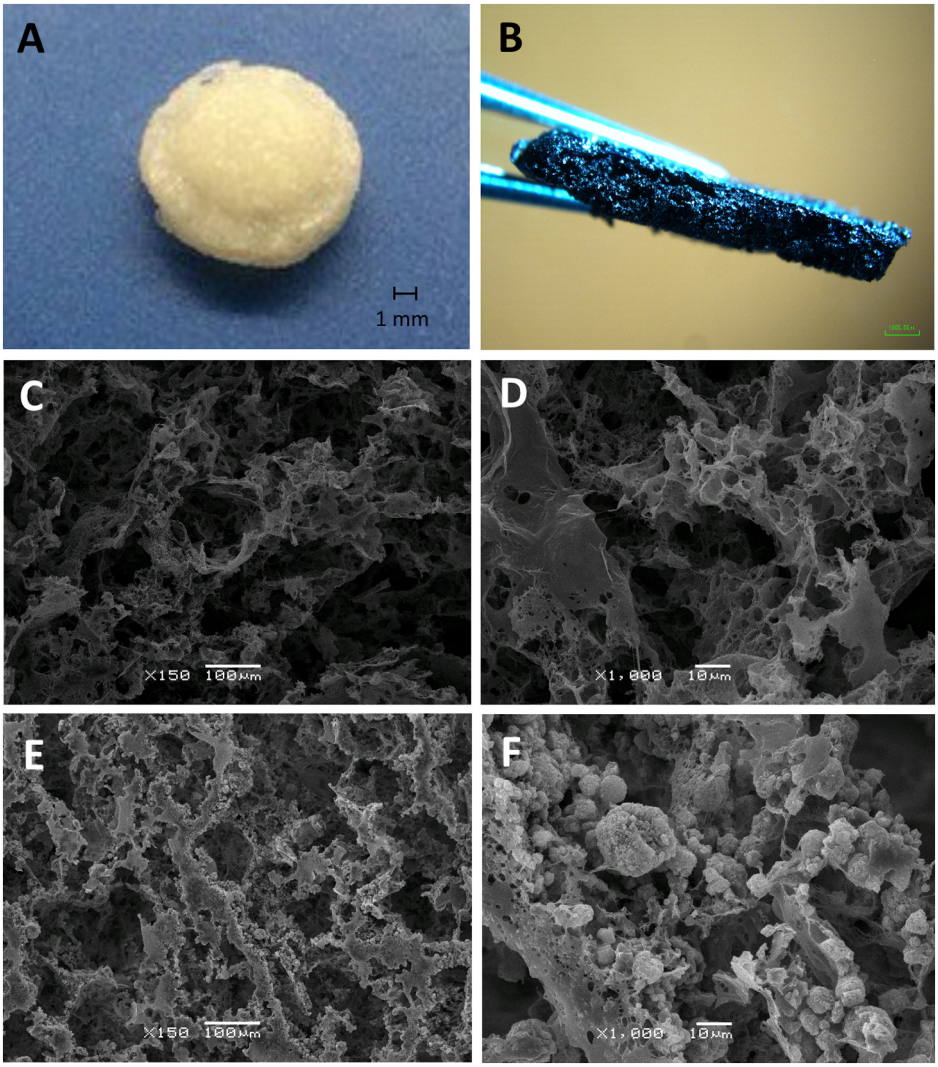

Fig. 1. Appearance and microstructure of PHB and PHB/HA porous scaffolds. A: an appearance of PHB scaffold; B: a microphotography of PHB scaffold with ink testing; C and D: the pore structure of PHB scaffold, SEM, ×150 (C), ×1000 (D); the pore structure of PHB/HA scaffold, SEM, ×150 (E), ×1000 (F).

channel fluorescence wide-angle image). New bone tissue formation was calculated as the area of newly formed bone tissue (in mm^2) [35].

2.7. Statistical analysis

The non-parametric Kruskal–Wallis test was employed for the statistical evaluation of data using the software package SPSS/PC+ Statistics™ 12.1 (SPSS). The obtained data were averaged with the standard error to the mean (± SD), and was considered significant for $p < 0.05$.

3. Results

3.1. Structure and morphology of scaffolds

The WFLM and SEM images of the produced PHB and PHB/HA scaffolds are shown in Fig. 1. As demonstrated by SEM, the PHB and PHB/HA scaffolds had a porous structure, the scaffold pores were of irregular shape with the microroughness of the pore walls (Fig. 1C, D, E, F). The ink test demonstrated that the PHB and PHB/HA scaffolds have an interconnected pore structure; there are no closed pores (that appear as white spots) in the obtained scaffold (Fig. 1B).

The average porosity and pore size are shown in Table 1. The produced PHB and PHB/HA scaffolds had a relatively high porosity (> 88%) and a pore size of about 100 μm. Blending PHB with HA caused a 5% decrease in porosity, and a 10% decrease in the pore size of produced scaffolds.

Table 1
Porosity and pore size of PHB and PHB/HA scaffolds.

The type of scaffold	Porosity, %	Size of pores, μm
PHB	93 ± 5	116 ± 26
PHB/HA	88 ± 6	104 ± 25

At the next stage of scaffold development, we filled the obtained PHB and PHB/HA porous scaffolds with ALG hydrogel, which is expected to be further used as a carrier for MSCs to encapsulate the cells into the PHB/HA scaffold. The microstructure of the empty PHB/HA scaffold and the produced composite PHB/HA/ALG scaffold are shown in Fig. 2.

The microscopy observation showed that the ALG hydrogel completely fills the pores of the scaffolds and lines the scaffolds from the outside.

3.2. Physicochemical properties of scaffolds

The mechanical properties of the obtained scaffolds varied greatly

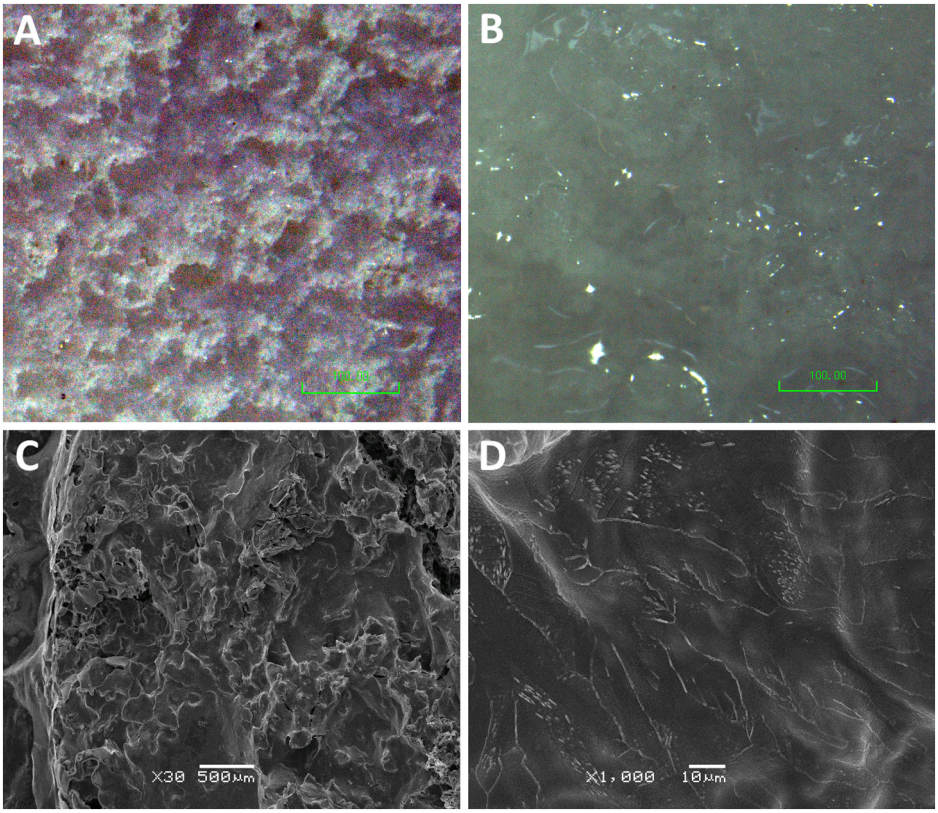

Fig. 2. Microstructure of PHB/HA scaffolds before (A) and after (B, C, D) filling with alginate hydrogel. A and B: WFLM, ×75; C: SEM, ×30; D: SEM, ×1000.

(Table 2). The Young's and Shear moduli of scaffolds from composites of PHB with HA are greater than those of scaffolds without hydroxyapatite. Similarly, the scaffolds filled with ALG hydrogel have a much higher Young's modulus than scaffolds that are not filled with ALG, e.g., PHB/HA/ALG scaffolds had five and 20 times higher Young's modulus compared with PHB/HA and PHB scaffolds, respectively. The Young modulus of ALG hydrogel itself was 19.2 kPa.

The parameters of thermo-physical properties calculated from the thermograms of scaffolds are also presented in Table 2. The melting temperature and crystallinity degree of the scaffold from the PHB/HA composite do not change significantly compared with the scaffold based on PHB. Meanwhile, the filling of the scaffold with ALG hydrogel led to a significant change in the thermogram; at low temperatures, the additional broad peak appears, which apparently reflects the process of evaporation of water from the ALG hydrogel and the thermal decomposition of ALG. These processes distort the entire thermogram, affecting the remaining melting peak of PHB at high temperatures. Thermograms of the obtained composite scaffolds are shown in Supplemental materials, Fig. S4. PHB blending with HA and filling the scaffolds with ALG hydrogel led to a significant decline in the degree of crystallinity of the produced PHB/HA/ALG scaffolds; it was 32% and 36% compared with PHB/HA and PHB scaffolds, respectively.

The study of the scaffold hydrophilicity by measuring their water uptake showed that PHB/HA scaffolds had relatively higher hydrophilicity compared with PHB scaffolds (Table 2). Indirectly, an increase in the hydrophilicity of PHB/HA scaffolds is indicated by a greater ability to adsorb protein to the polymer surface of scaffold pores (Supplemental materials, Fig. S5) [49,50], as well as a lower contact angle value of films made of composite PHB with HA (Supplemental materials, Table S1). Filling scaffolds with ALG hydrogel dramatically increased their hydrophilicity; the rise in water uptake was 65 and 100 times larger than that of PHB/HA and PHB scaffolds, respectively (Table 2).

3.3. Cell growth in scaffolds

First, to prove that the MSCs isolated from rat bone marrow are really mesenchymal stem cells, we conducted phenotyping of the obtained stem cells. The flow cytometry analysis showed that the fractions of positive and negative markers of MSC phenotype were as follows: CD 29–50%, CD 90–95%, CD11b/c – 26%, and CD 45–2%, thereby indicating their ability to adhere to culture plastic, enabling them to be characterized as MSCs [32]. The number of living cells was 98.8 ± 0.8% of the total (Supplemental materials, Fig. S1).

Cell viability testing was used to estimate the attachment and cell proliferation of MSCs in the PHB and PHB/HA scaffolds compared with MSC proliferation in ALG hydrogel and on TCPS. As indicated in Fig. 3, the cell proliferation in the PHB and PHB/HA scaffolds was much lower than on TCPS. MSC growth in spheres of ALG hydrogel was significantly lower than on TCPS, but also much higher than in both PHB and PHB/

Table 2
Physicochemical properties of the obtained scaffolds.

The scaffold	Young's modulus, kPa	Shear modulus, kPa	Melting temperature, T_m^{peak}, °C	Crystallinity degree, X_c, %	Water uptake, %
PHB	8.7 ± 0.1	54.2 ± 2.2	175	64.3 ± 1.2	2.4 ± 0.8
PHB/HA	34.0 ± 0.6	85.6 ± 3.0	177	60.2 ± 1.4	3.7 ± 1.3
PHB/ALG	42.0 ± 0.8	66.7 ± 2.1	176	45.9 ± 0.9	226 ± 23
PHB/HA/ALG	178.5 ± 1.8	254.3 ± 3.7	178	41.1 ± 0.7	241 ± 21

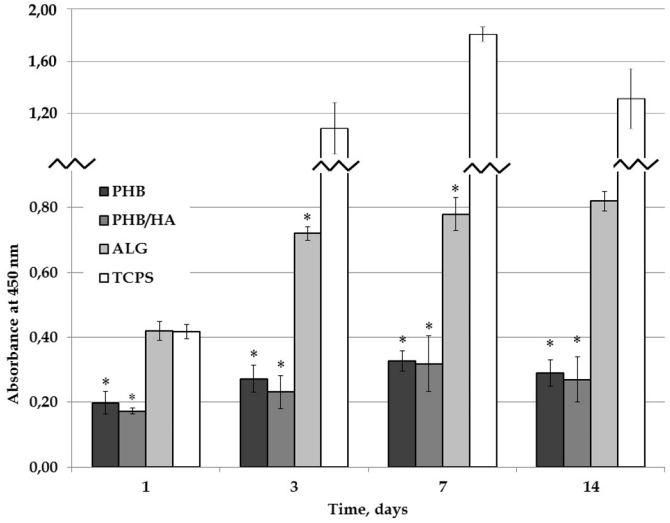

Fig. 3. Growth of MSCs in PHB scaffolds, PHB/HA scaffolds, and ALG hydrogel for 7 days. * $p < 0.05$ vs. TCPS; # $p < 0.05$ PHB and PHB/HA vs. ALG.

HA scaffolds. No significant difference was observed in MSC growth of PHB and PHB/HA scaffolds.

3.4. Alkaline phosphates activity and CD45 expression

To verify that the observed suppressed growth of MSCs may be caused by their differentiation, we measured the ALP activity and the expression level of the phenotype marker CD45 in MSCs on days 7, 14, and 21 of cultivation in the PHB and PHB/HA scaffolds in the regular medium (Fig. 4). We proposed that the reduced growth of MSCs in the scaffolds may be associated with a spontaneous osteogenic differentiation of stem cells. The significant increase in ALP activity in MSCs grown in PHB and PHB/HA scaffolds (2.7- and 4.6-fold, respectively, compared with cells grown on TCPS) and (indirectly) in the expression of the CD45 phenotype marker (1.9- and 12.2-fold, respectively, compared with MSCs grown on TCPS) indicates the spontaneous differentiation of MSCs in PHB and PHB/HA scaffolds in a regular medium starting from day 7 of cell cultivation. This is accompanied by a reduced growth of cells, in contrast to ALG hydrogel [36,40,42,51]. In an osteogenic medium, such a significant difference in ALP activity between MSCs grown in PHB or PHB/HA scaffolds and in ALG hydrogel or on TCPS was not observed (Supplemental materials, Fig. S6).

3.5. CT imaging

We examined the parietal bone using a CT scan to evaluate the bone regeneration. Twenty eight days after surgery, control empty defects showed minor healing, with a bone regeneration of only 10%. The bone defects filled with the acellular PHB/ALG, PHB/HA/ALG, or MSC-seeded PHB/HA/ALG/MSC scaffolds demonstrated a progressive amount of new bone formation, starting from the edges of the defect. No pronounced inflammation was observed in the area of implantation of the acellular and MSC-seeded scaffolds. Radiographic images (sagittal, transverse, and coronal slices) of the healing process of representative animals and analysis of the remodeled bone defect area are shown in Fig. 5. Scaffolds seeded with MSCs demonstrated a nearly complete coverage of the critical-sized parietal bone defect (% coverage of initial defect of 93.9 ± 4.4); the CT scan with maximal covering (98.3%) is shown in Fig. 5D, and the CT scan with minimal covering (89.6%) of bone defect in PHB/HA/ALG/MSC group is shown in Supplemental materials, Fig. S5. The use of acellular PHB/ALG and PHB/HA/ALG scaffolds caused only partial regeneration of the critical-sized defect of parietal bone: 37.0 ± 5.9% and 60.1 ± 6.2%, respectively.

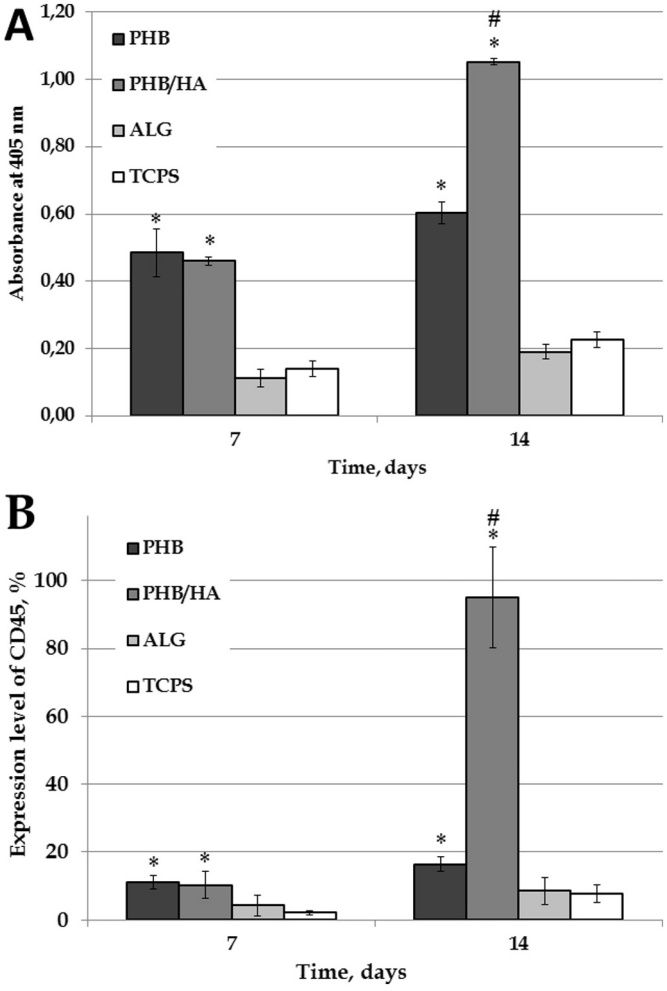

Fig. 4. ALP activity (A) and CD45 expression level (B) in MSCs on the 7th and 14th days of cell cultivation in PHB, PHB/HA, and ALG hydrogel in regular cultural medium. * $p < 0.05$ vs. TCPS; # $p < 0.05$ PHB and PHB/HA vs. ALG.

3.6. Histology and histomorphometry

The obtained histological evidence further supported the CT findings, indicating that MSC-seeded PHB/HA/ALG/MSC scaffolds demonstrated a progressive presence of newly formed mineralized bone tissue within the remodeled defect. A disk of scaffold material with a porous structure lies above the defect and is surrounded by connective tissue. Underneath it, the growth of the newly formed bone from the edges of the critical defect was observed. The newly formed bone had a typical organized and mature bone morphology with a lamellar structure in the form of wide layers, the thickness of which was comparable to the thickness of the old bone. While we did not reveal the complete overlap of the defect by the newly formed bone, in most cases, there was a convergence and merging of the fronts of the regenerates from the edges of the defects (Fig. 6D). In contrast, histological analysis indicated the formation of less bone in the critical defect area when using acellular PHB/ALG and PHB/HA/ALG scaffolds (Fig. 6B, C). The percentage of new mineralized bone tissue visualized with trichrome blue area was significantly higher ($p < 0.01$) when using MSC-seeded scaffolds (92%), compared to acellular PHB/ALG scaffolds (27%) on day 28 post surgery (Fig. 6E). It should be noted that the in vitro enzymatic degradation of PHB and PHB/HA base-scaffolds is relatively slow: scaffold mass loss becomes noticeable only after 6 months. However, for 1 month, there is a significant increase in the stiffness and hydrophilicity of these scaffolds (Supplemental materials, Fig. S9) [52].

The examination of the critical bone defect area using fluorescent

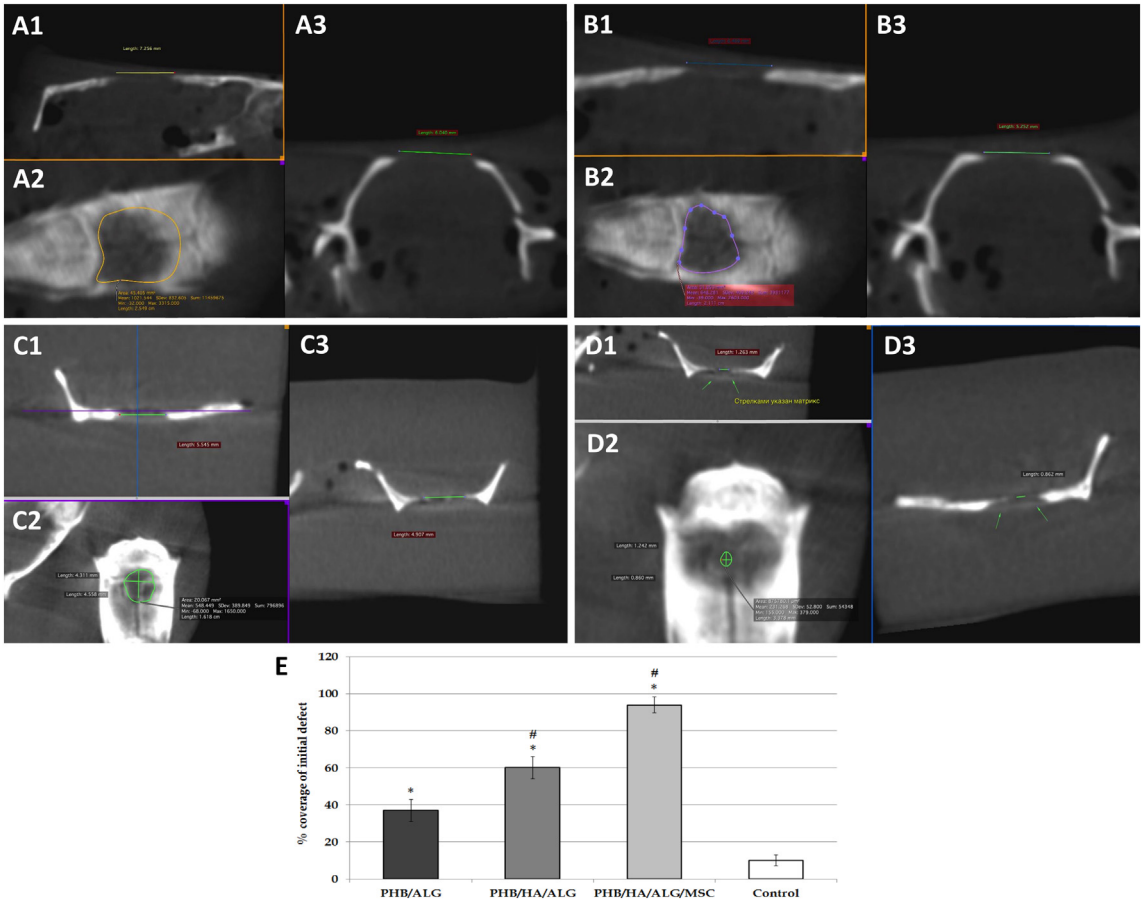

Fig. 5. CT images (sagittal (1), transverse (2), and coronal (3) slices) of the critical-sized radial defect of parietal bone in rat 28 days post implantation of acellular PHB/ALG (B) and PHB/HA/ALG (C), and MSC-seeded PHB/HA/ALG/MSC (D) scaffolds in comparison with empty control (A); corresponding data on % covering of initial defect (E) (* $p < 0.05$ vs. TCPS, # $p < 0.05$ vs. PHB/ALG scaffold). The bone defect was nearly completely covered by a bony flap 1 month after implantation of PHB/HA/ALG/MSC scaffold (indicated by green arrows) and partially covered after implantation of PHB/ALG and PHB/HA/ALG scaffolds in comparison with nearly non-regenerated defect in empty control. (For interpretation of the references to color in this figure legend, the reader is referred to the web version of this article.)

microscopy showed the dynamics of bone tissue regeneration due to the successful accumulation of fluorescent markers in the newly formed bone tissue at three different periods: 1–14 days (accumulation of doxycycline, yellow staining), 15–21 days (accumulation of tetracycline, green staining), and 22–28 days (accumulation of alizarin red, red staining); the blue color characterizes the background luminescence of ostein without fluorescent labels. After the implantation of MSC-seeded PHB/HA/ALG/MSC scaffolds, the main amount of bone tissue was formed at 22–28 days (red staining) (Fig. 7D), whereas the formation of new bone after the implantation of acellular PHB/ALG and PHB/HA/ALG scaffolds was practically not observed during this period, which indicates a decrease in the regeneration of the bone tissues of the parietal bones approximately three weeks after injury without an additional impact. The main bone area for PHB/ALG and PHB/HA/ALG scaffolds was stained with tetracycline (green staining), which indicates a predominant osteogenesis for a period of 14 to 21 days (Fig. 7B, C). However, the amount of newly formed bone after MSC-seeded scaffolds was significantly higher at all stages of the bone defect healing process compared with the use of PHB/ALG and PHB/HA/ALG scaffolds (Fig. 7E). Therefore, the total area of the regenerated bone tissue in critical-sized defects covered by PHB/HA/ALG/MSC scaffolds was much higher compared with scaffolds containing no MSCs (Fig. 7E). Thus, the implantation of MSC-seeded scaffolds showed the manifested stimulation of the reparative osteogenesis, with an increase in the initial area occupied by a bone regenerate on the surface of the dura mater.

4. Discussion

In this research we demonstrate that scaffolds based on PHB and its blend with HA filled both with ALG hydrogel caused partial bone regeneration in a critical-sized calvarial defect model in rats for 1 month. Further, these composite scaffolds combined with bone marrow MSCs drastically increased bone healing, indicating that such hybrid scaffolds represent a promising therapeutic tool to regenerate craniofacial bones. Moreover, it should be noted that bone reconstruction is particularly difficult for the craniofacial area, which is highly vulnerable to bone loss or defects because of trauma, infectious, inflammatory, and cancer-related diseases, or hereditary abnormalities.

The experimental models of critical-sized bone defects are currently the reference models employed with determining the efficiency of osteoconductive and osteoinductive biomaterials on bone healing and regeneration [44]. A bone defect with a diameter ranging from 5 to 8 mm was described as the critical-size defect in rats [45,46]. Therefore, a defect with a diameter of 8 mm, which is the upper limit of this range, was used to ensure that a critical-size defect is a highly reproducible experimental model.

We assume that the effect of developed hybrid scaffolds on bone tissue regeneration in the critical-sized calvarial defect model has a complex and multiple nature, and includes the interdependent influence of the main features of these constructions: their morphology, properties of their constituent biomaterials, and bioactivity of the MSCs itself.

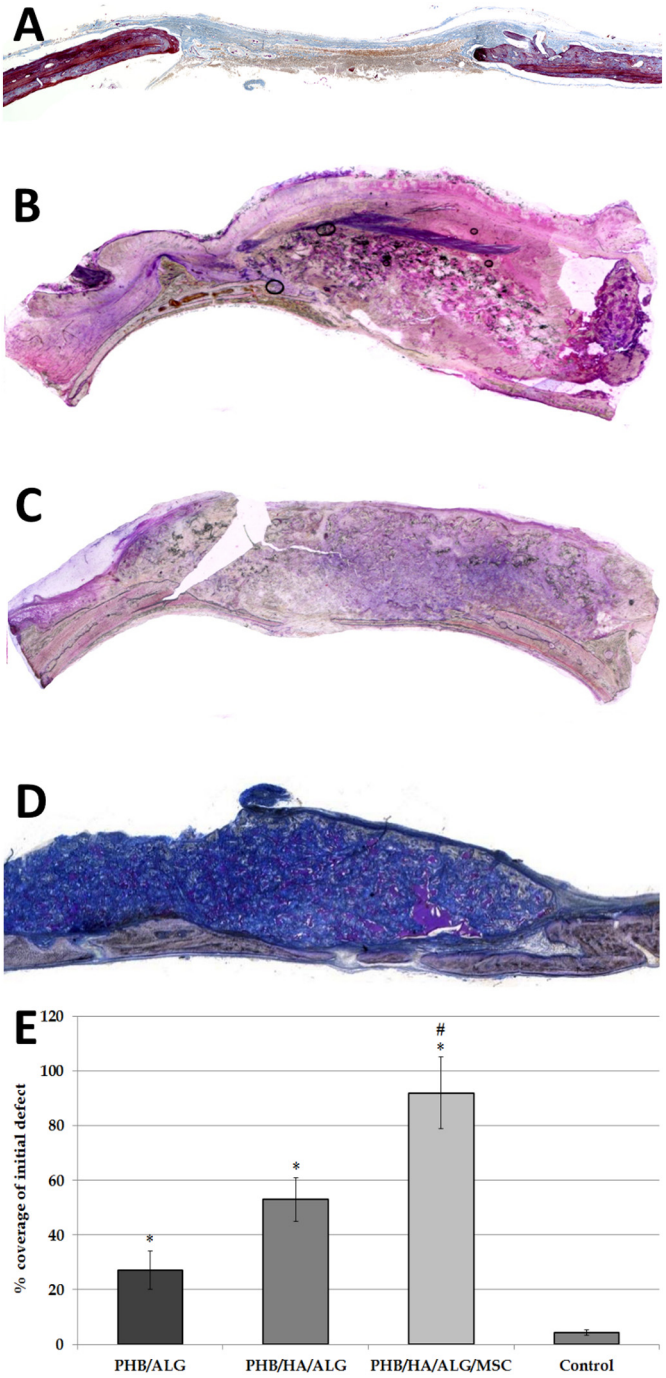

Fig. 6. Representative cross sections (wide-angle images) of the critical-sized radial defect of parietal bone in rat 28 days post implantation of acellular PHB/ALG (B), PHB/HA/ALG (C), and MSC seeded PHB/HA/ALG/MSC (D) scaffolds in comparison with empty control (A); and corresponding data on % covering of initial defect (D). Original trichrome blue staining (orange G, eosin, toluidine blue, basic fuchsin); (* $p < 0.05$ vs. TCPS, # $p < 0.05$ vs. PHB/ALG scaffold). (For interpretation of the references to color in this figure legend, the reader is referred to the web version of this article.)

The production of scaffolds from a PHB composite with HA and the filling of the scaffold with ALG hydrogel led to a significant increase in their mechanical strength. The definition of composite is following: "A structural composite is a material system consisting of two or more phases on a macroscopic scale, whose mechanical performance and properties are designed to be superior to those of the constituent materials acting independently. One of the phases is usually discontinuous, stiffer, and stronger and is called the reinforcement, whereas the less stiff and weaker phase is continuous and is called the matrix" [15]. Thus, since PHB/ALG and PHB/HA/ALG scaffolds are much stiffer than PHB and PHB/HA scaffolds, respectively, as well as ALG hydrogel (Table 2), we are entitled to consider them as true composites. The obtained PHB/HA/ALG scaffold can be defined as complex multi-directional continuous fiber composites [15], in which the reinforcement and the matrix would be represented by completely different materials in their physicochemical properties: PHB/HA particulate composite and ALG hydrogel. Indirectly, a similar cumulative effect of materials on each other can be seen from the analysis of scaffolds by DSC method (Table 2, Fig. S4) but DSC as well as FTIR can't show a chemical interaction between components in PHA/ALG composites [53].

The 3D microstructure of scaffolds contributes to the support of the growth of encapsulated MSCs and can also play the role of a guide for the cells of the body's own bone tissue, i.e., osteoclasts and osteoblasts. The interconnected pore structure and high porosity are key features for scaffolds used for bone tissue regeneration [8,36,37,42]. The scaffolds of the mean pore with sizes ranging from 20 μm to 1500 μm were used for the regeneration of bone defects [36,54,55]. It was shown that the minimal pore size for cell growth and bone tissue regeneration is about 40 μm, and the optimum range is about 100–200 μm [4,8,55,56]. It was also shown that a topography of polymer surface and a pore microstructure of scaffolds significantly influence not only the MSC growth but also cell differentiation in osteogenic, chondrogenic, and lipogenic directions [4,9,30]. A major role in the growth and differentiation of stem cells is also played by the physicochemical properties of the polymer biomaterials that are used for cell cultivation [30,41,57,58]. The physicochemical properties of produced composite scaffolds, namely the relatively low rigidity and combination of hydrophilic biomaterials (ALG hydrogel, HA) with hydrophobic biomaterials (PHB), can also improve the guiding properties for MSCs, osteoblasts, and osteoclasts for the better integration of scaffold with surrounding tissues with following induction of osteogenesis [38,59–62]. It should be considered that even the maximum values of the Young's modulus for the obtained scaffolds were many times less than the Young's modulus of the polymer material itself (the Young's modulus of the PHB is > 1500 MPa) and the bone tissue itself (the Young's modulus of the cancerous bone tissue is up to 500 MPa) [63]. Therefore, these scaffolds can be used only as a biomaterial for bone tissue regeneration, but not to ensure or replenish its biomechanical properties in the case of bone damage [4,8,10]. The main purpose of our research was not to use PHB/HA/ALG/MSC scaffold as a prosthesis for the critical-sized bone defect, but use it as the osteoinductive biomaterial to stimulate bone regeneration in this defect.

The biomaterials of scaffolds play a key role in their ability to promote bone regeneration. It was demonstrated that PHB and its co-polymers display the osteoinductive properties in vivo when scaffolds derived from these polymers were used as bone-substituting biomaterials and were implanted into bone defects. It was shown that porous scaffolds from PHB promote bone tissue regeneration, which was demonstrated in experimental models of critical (parietal bone of the rat skull) and noncritical (rat femur) bone defects [9,64]. At all stages of the process of bone defect regeneration, a minimally pronounced tissue reaction to implantation was observed. This reaction was associated with the gradual bioresorption of the polymeric material by osteoclasts, active vascularization of the scaffolds, and sprouting of the newly formed bone tissue into the pores of the PHB scaffolds (Supplemental materials, Fig. S10). The regeneration of bone tissue in the PHB scaffolds was also indicated by the expression of osteogenic markers, e.g., collagen type I. A high level of vascularization (angiogenesis) was demonstrated in the tissue defect area during regeneration while using PHB devices [28,42,65,66]. It was shown that HA has pronounced osteoinductive activity [67,68]. In our study, the osteoinductive activity was shown both for PHB/ALG scaffolds and composite PHB/HA/ALG

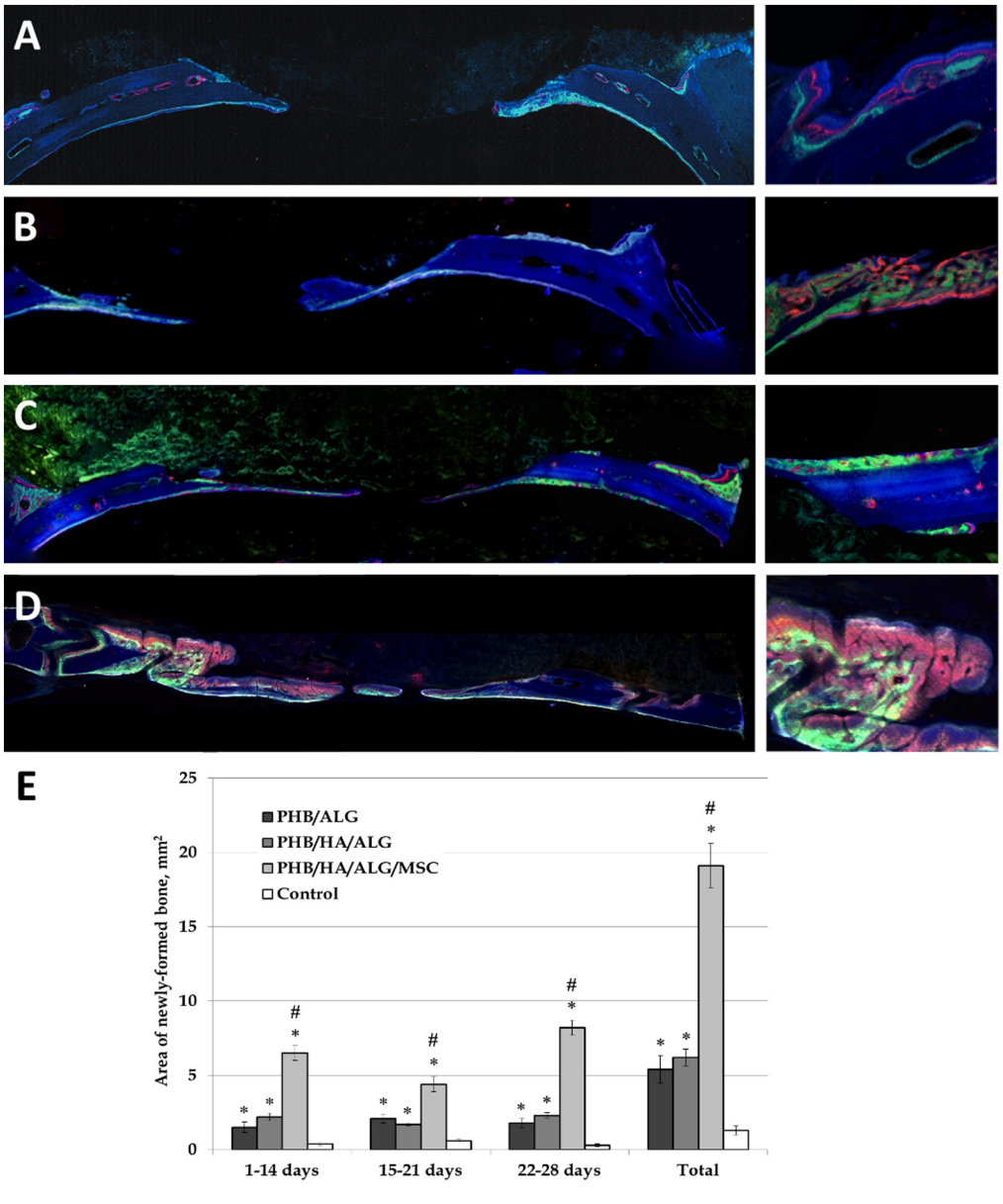

Fig. 7. Representative cross sections (multi-channel fluorescence wide-angle images) of the critical-sized radial defect of parietal bone in rat 28 days post implantation of acellular PHB/ALG (B), PHB/HA/ALG (C), MSC-seeded PHB/HA/ALG/MSC (D) scaffolds, control defect without scaffold (A), and quantification of newly formed bone tissue (E). The administration of fluorescent marks: doxycycline, tetracycline, and alizarine red C to rats was performed to visualize the newly formed bone tissue at different periods: 1–14 days, 15–21 days, and 22–28 days, respectively, when using multichannel fluorescent microscopy (# $p < 0.05$ vs. PHB/ALG scaffold). (For interpretation of the references to color in this figure legend, the reader is referred to the web version of this article.)

scaffolds. The HA-containing acellular PHB/HA/ALG scaffolds caused greater bone regeneration in the critical-sized defect model compared with the PHB/ALG scaffold (Fig. 5).

The osteoinductive activity of PHB/HA/ALG scaffolds in the regeneration of bone tissue in vivo may be associated with the ability of the PHB/HA composite to induce the osteogenic differentiation of MSCs in vitro. Here, we showed the differentiation of MSCs grown in PHB/HA scaffolds in a regular medium. PHB/HA scaffolds induced a pronounced increase in ALP activity and CD45 expression (Fig. 4). Such a spontaneous differentiation of MSCs in a regular medium or the stimulation of osteogenic differentiation of MSCs in an osteogenic medium was demonstrated not only for composite PHA/HA scaffolds [20–22,43], composite scaffolds from calcium phosphate cement, alginate, and methylcellulose [69] but even for the scaffolds from pure PHAs [40–43,51]. Scaffolds from composites of PHB with nano-bioglass were also demonstrated to induce elevated ALP activity in MG63 osteoblast-like cells grown on them in a regular medium [17,18]. Moreover, the formation of a surface apatite (Ca—P) layer on PHB and PHB/HA scaffolds during their incubation in simulated body liquid may be used as a test for scaffold bioactivity evaluation [7,17].

Hydrogels, e.g., ALG hydrogel, are also used for bone tissue engineering, but mainly as carriers for cells and bioactive substances [25,38,59,61,70,71]. We used ALG hydrogel as a carrier for MSC encapsulation and concentration in polymer scaffolds because this neutral substance is widely used for the encapsulation of various cells [5,72,73]. It was shown that the half-life of the dense alginate hydrogel after its intramuscular implantation is about 4 days [74]. The exchange of cross-linking calcium cations with monovalent sodium cations is the main cause of dissolution of calcium cross-linked alginate hydrogel [75,76] with the dramatic loss of its mechanical strength: it was shown that the shear modulus of alginate hydrogel decreased from 155 kPa to 5 kPa within 2 days [77]. Thus, after the implantation of PHB/ALG, PHB/HA/ALG, and PHB/HA/ALG/MSC scaffolds, the dense alginate hydrogel is kept only for several days. At the same time, as we propose, the proliferation of the encapsulated MSCs can occur in the pores of the PHB/HA base-structure of PHB/HA/ALG/MSC scaffold as it was shown in vitro (Fig. 3). And later the germination of the implanted scaffolds with gradual replacement of alginate hydrogel by newly formed bone tissue occurs (Figs. 6 and 7).

However, the noteworthy feature here is that the most effective regeneration of critical-sized bone defect was achieved using MSC-seeded composite scaffolds (Figs. 5, 6, and 7). After the implantation of

MSC-seeded PHB/HA/ALG/MSC scaffolds, the main amount of bone tissue was formed at days 22–28 (red staining) (Fig. 7D), whereas the newly formed bone after the implantation of acellular PHB/ALG and PHB/HA/ALG scaffolds was practically not observed during this period. This indicates a decrease in the regeneration of the bone tissues of the parietal bones approximately week 3 after injury without any additional impact. It is unknown whether encapsulated MSCs directly built new bone tissue or whether they initiated a natural regeneration cascade, which is comparable to autologous bone grafts, but the observed delayed osteogenic action of MSC-seeded scaffolds is believed to be related to the bioactivity of stem cells. We propose that MSCs encapsulated in scaffolds can promote bone regeneration by their stimulation using the polymer-mineral component of scaffolds and the production of cytokines and growth factors as well as by cell-to-cell interaction. This appears to be the most realistic explanation of the obtained data because we observed the bone regeneration mainly from the edges to the center of the defect (Figs. 6 and 7). It is also possible that at least some cells with stimulated osteogenic differentiation can migrate from the scaffold to the bone defect space, causing intercellular bone tissue matrix formation. This may explain the formation of bone islets (Figs. 6D and 7D) when using MSC-seeded scaffolds but they are absent in the case of acellular scaffolds.

5. Conclusions

The obtained results demonstrate that the biomimetic composite scaffolds from PHB/HA as reinforcement and ALG as a matrix can be used for the development of the hybrid MSC-seeded tissue engineering constructions for bone tissue regeneration. The developed technology combining indirect 3D printing and the porosity-control salt leaching method was shown as a promising approach to the manufacture scaffolds with a complex shape and structure that is friendly for MSC growth and bone tissue sprouting. Moreover, PHB/HA scaffolds were able to induce the osteogenic differentiation of MSCs. The original technique of living fluorescence labeling of newly forming bone tissue reveals 3-week postpone forming the main amount of bone tissue after the implantation of MSC-seeded PHB/HA/ALG scaffolds, whereas the newly formed bone after the implantation of acellular PHB/ALG and PHB/HA/ALG scaffolds is not observed during this period. This delayed osteogenic action of MSC-seeded scaffolds can be connected with the bioactivity of stem cells. Thus, the produced hybrid constructions based on PHB/HA scaffolds filled with MSC-containing ALG hydrogel enhance the regeneration and benefit bone regeneration process in the critical-sized radial defect of parietal bone in rats owing to both the possible osteoinductive properties of scaffolds and the regenerative potential of MSCs, which may appear when cells are encapsulated in composite biopolymer/mineral/hydrogel scaffolds. These results confirm the high potential of natural biomaterials, biomimetic structure scaffolds, and MSC-based approaches in tissue engineering for bone tissue regeneration.

CRediT authorship contribution statement

Alexey V. Volkov: Conceptualization, Investigation, Formal analysis, Writing - original draft. **Alexander A. Muraev**: Conceptualization, Investigation, Formal analysis, Writing - original draft. **Irina I. Zharkova**: Investigation. **Vera V. Voinova**: Investigation, Formal analysis. **Elizaveta A. Akoulina**: Investigation. **Vsevolod A. Zhuikov**: Investigation. **Dolgor D. Khaydapova**: Investigation. **Dariana V. Chesnokova**: Investigation. **Ksenia A. Menshikh**: Investigation. **Andrej A. Dudun**: Investigation. **Tatiana K. Makhina**: Investigation. **Garina A. Bonartseva**: Investigation, Writing - review & editing. **Teymur F. Asfarov**: Investigation. **Ivan A. Stamboliev**: Investigation. **Yulia V. Gazhva**: Investigation. **Valentina M. Ryabova**: Investigation. **Lubomir H. Zlatev**: Investigation. **Sergey Y. Ivanov**: Writing - review & editing. **Konstantin V. Shaitan**: Writing - review & editing. **Anton P. Bonartsev**: Conceptualization, Formal analysis, Writing - original draft.

Declaration of competing interest

The authors declare that they have no known competing financial interests or personal relationships that could have appeared to influence the work reported in this paper.

Acknowledgments

This work was supported by the Russian Science Foundation, project No 17-74-20104 (parts on scaffold characterization and MSC cultivation and study in scaffolds), by Russian Foundation for Basic Research, project No 18-29-09099 (parts on MSC cultivation and study in alginate hydrogel) and was carried out within the framework of government assignment (the part of poly(3-hydroxybutyrate) microbiological production by Azotobacter chroococcum 7B). The equipment used in this work was from the User Facilities Center of M.V. Lomonosov Moscow State University (including the FACSAria SORP complex, the scanning electron microscopes, Nano Spray Drier B-90, the facility system for the production of polymer micro- and nanoparticles etc.) and the User Facilities Center of Research Center of Biotechnology of Russian Academy of Sciences.

Appendix A. Supplementary data

Supplementary data to this article can be found online at https://doi.org/10.1016/j.msec.2020.110991.

References

[1] I.R. Murray, C.C. West, W.R. Hardy, A.W. James, T.S. Park, A. Nguyen, T. Tawonsawatruk, L. Lazzari, C. Soo, B. Péault, Natural history of mesenchymal stem cells, from vessel walls to culture vessels, Cell. Mol. Life Sci. 71 (2014) 1353–1374, https://doi.org/10.1007/s00018-013-1462-6.
[2] H.T. Liao, C.T. Chen, Osteogenic potential: comparison between bone marrow and adipose-derived mesenchymal stem cells, World J. Stem Cells. 6 (2014) 288–295, https://doi.org/10.4252/wjsc.v6.i3.288.
[3] N.K. Paschos, W.E. Brown, R. Eswaramoorthy, J.C. Hu, K.A. Athanasiou, Advances in tissue engineering through stem cell-based co-culture, J. Tissue Eng. Regen. Med. 9 (2015) 488–503, https://doi.org/10.1002/term.1870.
[4] A. Oryan, S. Alidadi, A. Moshiri, N. Maffulli, Bone regenerative medicine: classic options, novel strategies, and future directions, J. Orthop. Surg. Res. 9 (2014) 1–27, https://doi.org/10.1186/1749-799X-9-18.
[5] F. Sefat, M. Mozafari, A. Atala, Introduction to tissue engineering scaffolds, Handb. Tissue Eng. Scaffolds, One Elsevier, 2019, pp. 3–22, , https://doi.org/10.1016/B978-0-08-102563-5.00001-0.
[6] H. Hajiali, S. Karbasi, M. Hosseinalipour, H.R. Rezaie, Preparation of a novel biodegradable nanocomposite scaffold based on poly (3-hydroxybutyrate)/bioglass nanoparticles for bone tissue engineering, J. Mater. Sci. Mater. Med. 21 (2010) 2125–2132, https://doi.org/10.1007/s10856-010-4075-8.
[7] M. Zarei, S. Karbasi, Evaluation of the effects of multiwalled carbon nanotubes on electrospun poly(3-hydroxybutirate) scaffold for tissue engineering applications, J. Porous. Mater. 25 (2018) 259–272, https://doi.org/10.1007/s10934-017-0439-5.
[8] A. Houben, J. Van Hoorick, J. Van Erps, H. Thienpont, S. Van Vlierberghe, P. Dubruel, Indirect rapid prototyping: opening up unprecedented opportunities in scaffold design and applications, Ann. Biomed. Eng. 45 (2017) 58–83, https://doi.org/10.1007/s10439-016-1610-x.
[9] J. Lim, M. You, J. Li, Z. Li, Emerging bone tissue engineering via polyhydroxyalkanoate (PHA)-based scaffolds, Mater. Sci. Eng. C. 79 (2017) 917–929, https://doi.org/10.1016/j.msec.2017.05.132.
[10] K. Rezwan, Q.Z. Chen, J.J. Blaker, A.R. Boccaccini, Biodegradable and bioactive porous polymer/inorganic composite scaffolds for bone tissue engineering, Biomaterials 27 (2006) 3413–3431, https://doi.org/10.1016/j.biomaterials.2006.01.039.
[11] G. Wei, P.X. Ma, Polymeric biomaterials for tissue engineering, Tissue Eng. Using Ceram. Polym. Second Ed, Elsevier Inc, 2014, pp. 35–66, , https://doi.org/10.1533/9780857097163.1.35.
[12] M. González Torres, Polyurethane/urea composite scaffolds based on poly(3-hydroxybutyrate-g-2-amino-ethyl methacrylate), Compos. Part B Eng. 160 (2019) 362–368, https://doi.org/10.1016/j.compositesb.2018.12.090.
[13] A.P. Reyes, A. Martínez Torres, M.D.P. Carreón Castro, J.R. Rodríguez Talavera, S.V. Muñoz, V.M.V. Aguilar, M.G. Torres, Novel poly(3-hydroxybutyrate-g-vinyl

alcohol) polyurethane scaffold for tissue engineering, Sci. Rep. 6 (2016) 1–8, https://doi.org/10.1038/srep31140.
[14] M.G. Torres, 3D-composite scaffolds from radiation-induced chitosan grafted poly (3-hydroxybutyrate) polyurethane, Mater. Today Commun. 23 (2020), https://doi.org/10.1016/j.mtcomm.2020.100902.
[15] I.M. Daniel, I. Ori, Engineering Mechanics of Composite Materials, 2nd ed., (2006), https://doi.org/10.1016/B978-1-84569-385-5.50021-0.
[16] K. Zhao, Y. Deng, J.C. Chen, G.Q. Chen, Polyhydroxyalkanoate (PHA) scaffolds with good mechanical properties and biocompatibility, Biomaterials (2003), https://doi.org/10.1016/S0142-9612(02)00426-X.
[17] A. Saadat, A. Behnamghader, S. Karbasi, D. Abedi, M. Soleimani, A. Shafiee, Comparison of acellular and cellular bioactivity of poly 3- hydroxybutyrate/hydroxyapatite nanocomposite and poly 3-hydroxybutyrate scaffolds, Biotechnol. Bioprocess Eng. 18 (2013) 1–7, https://doi.org/10.1007/RESEARCH.
[18] H. Hajiali, M. Hosseinalipour, S. Karbasi, M.A. Shokrgozar, The influence of bioglass nanoparticles on the biodegradation and biocompatibility of poly (3-hydroxybutyrate) scaffolds, Int. J. Artif. Organs. 35 (2012) 1015–1024, https://doi.org/10.1177/039139881203501107.
[19] R. Iron, M. Mehdikhani, E. Naghashzargar, S. Karbasi, D. Semnani, Effects of nanobioactive glass on structural, mechanical and bioactivity properties of poly (3-hydroxybutyrate) electrospun scaffold for bone tissue engineering applications, Mater. Technol. 34 (2019) 540–548, https://doi.org/10.1080/10667857.2019.1591728.
[20] A.M.A. Ambrosio, J.S. Sahota, Y. Khan, C.T. Laurencin, A novel amorphous calcium phosphate polymer ceramic for bone repair: I. Synthesis and characterization, J. Biomed. Mater. Res. 58 (2001) 295–301, https://doi.org/10.1002/1097-4636(2001)58:3<295::AID-JBM1020>3.0.CO;2-8.
[21] S.-S. Kim, K.-M. Ahn, M.S. Park, J.-H. Lee, C.Y. Choi, B.-S. Kim, A poly(lactide-co-glycolide)/hydroxyapatite composite scaffold with enhanced osteoconductivity, J. Biomed. Mater. Res. Part A. 80 (2007) 206–215, https://doi.org/10.1002/jbm.a.30836.
[22] M. Degli Esposti, F. Chiellini, F. Bondioli, D. Morselli, P. Fabbri, Highly porous PHB-based bioactive scaffolds for bone tissue engineering by in situ synthesis of hydroxyapatite, Mater. Sci. Eng. C. 100 (2019) 286–296, https://doi.org/10.1016/j.msec.2019.03.014.
[23] M. González, U. Merino, S. Vargas, F. Quintanilla, R. Rodríguez, Synthesis and characterization of a HAp-based biomarker with controlled drug release for breast cancer, Mater. Sci. Eng. C. 61 (2016) 801–808, https://doi.org/10.1016/j.msec.2016.01.015.
[24] G.M. Luz, J.F. Mano, Mineralized structures in nature: examples and inspirations for the design of new composite materials and biomaterials, Compos. Sci. Technol. 70 (2010) 1777–1788, https://doi.org/10.1016/j.compscitech.2010.05.013.
[25] J. Venkatesan, I. Bhatnagar, P. Manivasagan, K.H. Kang, S.K. Kim, Alginate composites for bone tissue engineering: a review, Int. J. Biol. Macromol. 72 (2015) 269–281, https://doi.org/10.1016/j.ijbiomac.2014.07.008.
[26] A.P. Bonartsev, I.I. Zharkova, S.G. Yakovlev, V.L. Myshkina, T.K. Mahina, V.V. Voinova, A.L. Zernov, V.A. Zhuikov, E.A. Akoulina, E.V. Ivanova, E.S. Kuznetsova, K.V. Shaitan, G.A. Bonartseva, Biosynthesis of poly(3-hydroxybutyrate) copolymers by Azotobacter chroococcum 7B: a precursor feeding strategy, Prep. Biochem. Biotechnol. 47 (2017) 173–184, https://doi.org/10.1080/10826068.2016.1188317.
[27] Y. Ramot, M. Haim-Zada, A.J. Domb, A. Nyska, Biocompatibility and safety of PLA and its copolymers, Adv. Drug Deliv. Rev. 107 (2016) 153–162, https://doi.org/10.1016/j.addr.2016.03.012.
[28] A.P. Bonartsev, G.A. Bonartseva, I.V. Reshetov, K.V. Shaitan, M.P. Kirpichnikov, Application of polyhydroxyalkanoates in medicine and the biological activity of natural poly(3-hydroxybutyrate), Acta Nat. 11 (2019) 4–16, https://doi.org/10.32607/20758251-2019-11-2-4-16.
[29] E. Akoulina, A. Dudun, A. Bonartsev, G. Bonartseva, V. Voinova, Effect of bacterial alginate on growth of mesenchymal stem cells, Int. J. Polym. Mater. Polym. Biomater. 68 (2019) 115–118, https://doi.org/10.1080/00914037.2018.1525730.
[30] H.Y. Bai, G.A. Chen, G.H. Mao, T.R. Song, Y.X. Wang, Three step derivation of cartilage like tissue from human embryonic stem cells by 2D-3D sequential culture in vitro and further implantation in vivo on alginate/PLGA scaffolds, J. Biomed. Mater. Res. Part A. 94 (2010) 539–546, https://doi.org/10.1002/jbm.a.32732.
[31] K.-H. Sun, Z. Liu, C.-J. Liu, T. Yu, M. Zhou, C. Liu, F. Ran, L.-J. Pan, H. Zhang, In vivo study of alginate hydrogel conglutinating cells to polycaprolactone vascular scaffolds fabricated by electrospinning, J. Biomed. Mater. Res. Part B Appl. Biomater. 105 (2017) 2443–2454, https://doi.org/10.1002/jbm.b.33731.
[32] M.T. Harting, F. Jimenez, S. Pati, J. Baumgartner, C.S. Cox, Immunophenotype characterization of rat mesenchymal stromal cells, Cytotherapy 10 (2008) 243–253, https://doi.org/10.1080/14653240801950000.
[33] S.A. Boxall, E. Jones, Markers for characterization of bone marrow multipotential stromal cells, Stem Cells Int. 2012 (2012) 1–12, https://doi.org/10.1155/2012/975871.
[34] A.P. Bonartsev, I.I. Zharkova, V.V. Voinova, E.S. Kuznetsova, V.A. Zhuikov, T.K. Makhina, V.L. Myshkina, D.M. Potashnikova, D.V. Chesnokova, D.D. Khaydapova, G.A. Bonartseva, K.V. Shaitan, Poly(3-hydroxybutyrate)/poly (ethylene glycol) scaffolds with different microstructure: the effect on growth of mesenchymal stem cells, 3 Biotech 8 (2018) 328, https://doi.org/10.1007/s13205-018-1350-8.
[35] A.A. Muraev, A.P. Bonartsev, Y.V. Gazhva, V.M. Riabova, A.V. Volkov, I.I. Zharkova, I.A. Stamboliev, E.S. Kuznetsova, V.A. Zhuikov, V.L. Myshkina, T.K. Mahina, G.A. Bonartseva, S.G. Yakovlev, K.S. Kudryashova, V.V. Voinova, A.A. Mironov, K.V. Shaitan, S.I. Gazhva, S.Y. Ivanov, Development and preclinical studies of orthotopic bone implants based on a hybrid construction from poly(3-hydroxybutyrate) and sodium alginate, Sovrem. Tehnol. v Med. 8 (2016) 42–50, https://doi.org/10.17691/stm2016.8.4.06.
[36] Ł. Rumian, I. Wojak, D. Scharnweber, E. Pamuła, Resorbable scaffolds modified with collagen type I or hydroxyapatite: in vitro studies on human mesenchymal stem cells, Acta Bioeng. Biomech. Orig. Pap. 15 (2013) 61–67, https://doi.org/10.5277/abb130108.
[37] M.A. Nosenko, N.V. Maluchenko, M.S. Drutskaya, A.Y. Arkhipova, I.I. Agapov, S.A. Nedospasov, M.M. Moisenovich, Induction of ICAM-1 expression in mouse embryonic fibroblasts cultured on fibroin-gelatin scaffolds, Acta Nat. 9 (2017) 89–93 http://www.ncbi.nlm.nih.gov/pubmed/29104780.
[38] C.N. Salinas, K.S. Anseth, Mesenchymal stem cells for craniofacial tissue regeneration: designing hydrogel delivery vehicles, J. Dent. Res. 88 (2009) 681–692, https://doi.org/10.1177/0022034509341553.
[39] Z. Zheng, F. Bei, H. Tian, G. Chen, Effects of crystallization of polyhydroxyalkanoate blend on surface physicochemical properties and interactions with rabbit articular cartilage chondrocytes, Biomaterials 26 (2005) 3537–3548, https://doi.org/10.1016/j.biomaterials.2004.09.041.
[40] A.C.C. de Paula, A.A.C. Zonari, T.M. da M. Martins, S. Novikoff, A.R.P. da Silva, V.M. Correlo, R.L. Reis, D.A. Gomes, A.M. Goes, Human serum is a suitable supplement for the osteogenic differentiation of human adipose-derived stem cells seeded on poly-3-hydroxibutyrate-co-3-hydroxyvalerate scaffolds, Tissue Eng. Part A. 19 (2013) 277–289, https://doi.org/10.1089/ten.tea.2012.0189.
[41] S.N. Gorodzha, A.R. Muslimov, D.S. Syromotina, A.S. Timin, N.Y. Tcvetkov, K.V. Lepik, A.V. Petrova, M.A. Surmeneva, D.A. Gorin, G.B. Sukhorukov, R.A. Surmenev, A comparison study between electrospun polycaprolactone and piezoelectric poly(3-hydroxybutyrate-co-3-hydroxyvalerate) scaffolds for bone tissue engineering, Colloids Surfaces B Biointerfaces 160 (2017) 48–59, https://doi.org/10.1016/j.colsurfb.2017.09.004.
[42] A.A. Shumilova, M.P. Myltygashev, A.K. Kirichenko, E.D. Nikolaeva, T.G. Volova, E.I. Shishatskaya, Porous 3D implants of degradable poly-3-hydroxybutyrate used to enhance regeneration of rat cranial defect, J. Biomed. Mater. Res. Part A. 105 (2017) 566–577, https://doi.org/10.1002/jbm.a.35933.
[43] L.-X. Lü, X.-F. Zhang, Y.-Y. Wang, L. Ortiz, X. Mao, Z.-L. Jiang, Z.-D. Xiao, N.-P. Huang, Effects of hydroxyapatite-containing composite nanofibers on osteogenesis of mesenchymal stem cells in vitro and bone regeneration in vivo, ACS Appl. Mater. Interfaces 5 (2013) 319–330, https://doi.org/10.1021/am302146w.
[44] P.P. Spicer, J.D. Kretlow, S. Young, J.A. Jansen, F.K. Kasper, A.G. Mikos, Evaluation of bone regeneration using the rat critical size calvarial defect, Nat. Protoc. 7 (2012) 1918–1929, https://doi.org/10.1038/nprot.2012.113.
[45] J.P. Schmitz, J.O. Hollinger, The critical size defect as an experimental model for craniomandibulofacial nonunions, Clin. Orthop. Relat. Res. 205 (1986) 299–308, https://doi.org/10.1097/00003086-198604000-00036.
[46] C. Bosch, B. Melsen, K. Vargervik, Importance of the critical-size bone defect in testing bone-regenerating materials, J. Craniofac. Surg. 9 (1998) 310–316, https://doi.org/10.1097/00001665-199807000-00004.
[47] D.B. Burr, M.R. Allen, Basic and Applied Bone Biology, 2nd edition, (2013) https://www.elsevier.com/books/basic-and-applied-bone-biology/burr/978-0-12-813259-3 , Accessed date: 28 March 2020.
[48] Y.H. An, K.L. Martin (Ed.), Handbook of Histology Methods for Bone and Cartilage, Springer Science + Business Media, Humana Press, Totowa, NJ, 2003, , https://doi.org/10.1007/978-1-59259-417-7.
[49] P. Roach, D. Farrar, C.C. Perry, Interpretation of protein adsorption: surface-induced conformational changes, J. Am. Chem. Soc. 127 (2005) 8168–8173, https://doi.org/10.1021/ja042898o.
[50] H. Noh, E.A. Vogler, Volumetric interpretation of protein adsorption: mass and energy balance for albumin adsorption to particulate adsorbents with incrementally increasing hydrophilicity, Biomaterials 27 (2006) 5801–5812, https://doi.org/10.1016/j.biomaterials.2006.08.005.
[51] F.S. Hosseini, F. Soleimanifar, A. Aidun, S.E. Enderami, E. Saburi, H.Z. Marzouni, M. Khani, A. Khojasteh, A. Ardeshirylajimi, Poly (3-hydroxybutyrate-co-3-hydroxyvalerate) improved osteogenic differentiation of the human induced pluripotent stem cells while considered as an artificial extracellular matrix, J. Cell. Physiol. 234 (2019) 11537–11544, https://doi.org/10.1002/jcp.27807.
[52] V.A. Zhuikov, Y.V. Zhuikova, T.K. Makhina, V.L. Myshkina, A. Rusakov, A. Useinov, V.V. Voinova, G.A. Bonartseva, A.A. Berlin, A.P. Bonartsev, A.L. Iordanskii, Comparative structure-property characterization of poly(3-hydroxybutyrate-co-3-hydroxyvalerate)s films under hydrolytic and enzymatic degradation: finding a transition point in 3-hydroxyvalerate content, Polymers (Basel) 12 (2020) 728, https://doi.org/10.3390/polym12030728.
[53] H. Zhu, J. Ji, R. Lin, C. Gao, L. Feng, J. Shen, Surface engineering of poly(dl-lactic acid) by entrapment of alginate-amino acid derivatives for promotion of chondrogenesis, Biomaterials 23 (2002) 3141–3148, https://doi.org/10.1016/S0142-9612(02)00058-3.
[54] S.H. Oh, I.K. Park, J.M. Kim, J.H. Lee, In vitro and in vivo characteristics of PCL scaffolds with pore size gradient fabricated by a centrifugation method, Biomaterials 28 (2007) 1664–1671, https://doi.org/10.1016/j.biomaterials.2006.11.024.
[55] S.M. Richardson, J.M. Curran, R. Chen, A. Vaughan-Thomas, J.A. Hunt, A.J. Freemont, J.A. Hoyland, The differentiation of bone marrow mesenchymal stem cells into chondrocyte-like cells on poly-l-lactic acid (PLLA) scaffolds, Biomaterials 27 (2006) 4069–4078, https://doi.org/10.1016/j.biomaterials.2006.03.017.
[56] J.J. Klawitter, J.G. Bagwell, A.M. Weinstein, B.W. Sauer, J.R. Pruitt, An evaluation of bone growth into porous high density polyethylene, J. Biomed. Mater. Res. 10 (1976) 311–323, https://doi.org/10.1002/jbm.820100212.
[57] P. Humpolíček, K.A. Radaszkiewicz, V. Kašpárková, J. Stejskal, M. Trchová, Z. Kuceková, H. Vičarová, J. Pacherník, M. Lehocký, A. Minařík, Stem cell

differentiation on conducting polyaniline, RSC Adv. 5 (2015) 68796–68805, https://doi.org/10.1039/C5RA12218J.
[58] V.I. Kulikouskaya, S.V. Pinchuk, K.S. Hileuskaya, A.N. Kraskouski, I.B. Vasilevich, K.A. Matievski, V.E. Agabekov, I.D. Volotovski, Layer-by-layer buildup of polysaccharide-containing films: physico-chemical properties and mesenchymal stem cells adhesion, J. Biomed. Mater. Res. Part A. 106 (2018) 2093–2104, https://doi.org/10.1002/jbm.a.36408.
[59] T. Garg, O. Singh, S. Arora, R.S.R. Murthy, Scaffold: a novel carrier for cell and drug delivery, Crit. Rev. Ther. Drug Carr. Syst. 29 (2012) 1–63, https://doi.org/10.1615/CritRevTherDrugCarrierSyst.v29.i1.10.
[60] T. Jiang, G. Xu, X. Chen, X. Huang, J. Zhao, L. Zheng, Impact of hydrogel elasticity and adherence on osteosarcoma cells and osteoblasts, Adv. Healthc. Mater. 8 (2019) 1801587, , https://doi.org/10.1002/adhm.201801587.
[61] D.J. Munoz-Pinto, A.C. Jimenez-Vergara, Y. Hou, H.N. Hayenga, A. Rivas, M. Grunlan, M.S. Hahn, Osteogenic potential of poly(ethylene glycol)–poly(dimethylsiloxane) hybrid hydrogels, Tissue Eng. Part A. 18 (2012) 1710–1719, https://doi.org/10.1089/ten.tea.2011.0348.
[62] A.J. Lomas, G.G. Chen, A.J. El Haj, N. Forsyth, Poly(3-hydroxybutyrate-co-3-hydroxyhexanoate) supports adhesion and migration of mesenchymal stem cells and tenocytes, World J. Stem Cells. 4 (2012) 94–100, https://doi.org/10.4252/wjsc.v4.i9.94.
[63] A. Odgaard, F. Linde, The underestimation of Young's modulus in compressive testing of cancellous bone specimens, J. Biomech. 24 (1991) 691–698, https://doi.org/10.1016/0021-9290(91)90333-I.
[64] A.P. Bonartsev, Poly(3-hydroxybutyrate): applications, in: M. Mishra (Ed.), Encycl. Polym. Appl, CRC Press, Taylor and Francis Group, Boca Raton, 2019, pp. 2061–2076, , https://doi.org/10.1201/9781351019422-140000085.
[65] C. Rentsch, B. Rentsch, A. Breier, A. Hofmann, S. Manthey, D. Scharnweber, A. Biewener, H. Zwipp, Evaluation of the osteogenic potential and vascularization of 3D poly(3)hydroxybutyrate scaffolds subcutaneously implanted in nude rats, J. Biomed. Mater. Res. Part A. 92 (2010) 185–195, https://doi.org/10.1002/jbm.a.32314.
[66] A.C.C. Paula, P.H. Carvalho, T.M.M. Martins, J.N. Boeloni, P.S. Cunha, S. Novikoff, V.M. Correlo, R.L. Reis, A.M. Goes, Improved vascularisation but inefficient in vivo bone regeneration of adipose stem cells and poly-3-hydroxybutyrate-co-3-hydroxyvalerate scaffolds in xeno-free conditions, Mater. Sci. Eng. C. 107 (2020) 110301, , https://doi.org/10.1016/j.msec.2019.110301.
[67] X. Shi, K. Zhou, F. Huang, J. Zhang, C. Wang, Endocytic mechanisms and osteoinductive profile of hydroxyapatite nanoparticles in human umbilical cord Wharton's jelly-derived mesenchymal stem cells, Int. J. Nanomedicine 13 (2018) 1457–1470, https://doi.org/10.2147/IJN.S155814.
[68] J. Jeong, J.H. Kim, J.H. Shim, N.S. Hwang, C.Y. Heo, Bioactive calcium phosphate materials and applications in bone regeneration, Biomater. Res. 23 (2019) 4, https://doi.org/10.1186/s40824-018-0149-3.
[69] T. Ahlfeld, N. Cubo-Mateo, S. Cometta, V. Guduric, C. Vater, A. Bernhardt, A.R. Akkineni, A. Lode, M. Gelinsky, A novel plasma-based bioink stimulates cell proliferation and differentiation in bioprinted, mineralized constructs, ACS Appl. Mater. Interfaces 12 (2020) 12557–12572, https://doi.org/10.1021/acsami.0c00710.
[70] R. Mhanna, A. Kashyap, G. Palazzolo, Q. Vallmajo-Martin, J. Becher, S. Möller, M. Schnabelrauch, M. Zenobi-Wong, Chondrocyte culture in three dimensional alginate sulfate hydrogels promotes proliferation while maintaining expression of chondrogenic markers, Tissue Eng. Part A. 20 (2014) 1454–1464, https://doi.org/10.1089/ten.tea.2013.0544.
[71] G. Apte, A. Repanas, C. Willems, A. Mujtaba, C.E.H. Schmelzer, A. Raichur, F. Syrowatka, T. Groth, Effect of different crosslinking strategies on physical properties and biocompatibility of freestanding multilayer films made of alginate and chitosan, Macromol. Biosci. 19 (2019) 1900181, , https://doi.org/10.1002/mabi.201900181.
[72] A.S. Hoffman, Hydrogels for biomedical applications, Adv. Drug Deliv. Rev. 54 (2002) 3–12, https://doi.org/10.1016/S0169-409X(01)00239-3.
[73] W.-H. Tan, S. Takeuchi, Monodisperse alginate hydrogel microbeads for cell encapsulation, Adv. Mater. 19 (2007) 2696–2701, https://doi.org/10.1002/adma.200700433.
[74] T.V. Shkand, M.O. Chizh, I.V. Sleta, B.P. Sandomirsky, A.L. Tatarets, L.D. Patsenker, Assessment of alginate hydrogel degradation in biological tissue using viscosity-sensitive fluorescent dyes, Methods Appl. Fluoresc. 4 (2016) 044002, , https://doi.org/10.1088/2050-6120/4/4/044002.
[75] K.Y. Lee, D.J. Mooney, Alginate: properties and biomedical applications, Prog. Polym. Sci. 37 (2012) 106–126, https://doi.org/10.1016/j.progpolymsci.2011.06.003.
[76] M. Matyash, F. Despang, C. Ikonomidou, M. Gelinsky, Swelling and mechanical properties of alginate hydrogels with respect to promotion of neural growth, Tissue Eng. Part C Methods. 20 (2014) 401–411, https://doi.org/10.1089/ten.tec.2013.0252.
[77] D. Shahriari, J. Koffler, D.A. Lynam, M.H. Tuszynski, J.S. Sakamoto, Characterizing the degradation of alginate hydrogel for use in multilumen scaffolds for spinal cord repair, J. Biomed. Mater. Res. Part A. 104 (2016) 611–619, https://doi.org/10.1002/jbm.a.35600.